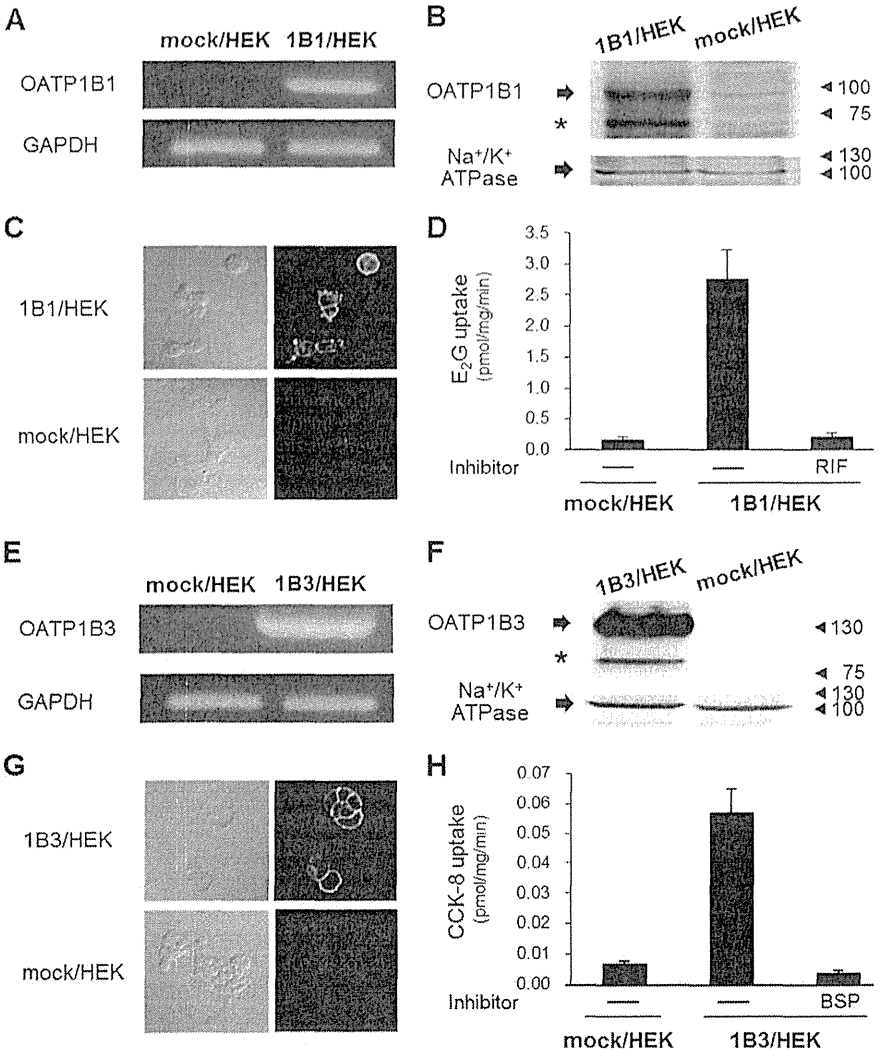

FIG 1 Functional expression of OATP1B1 or OATP1B3 in HEK293 cells. (A and E) RT-PCR was performed to examine OATP1B1 or OATP1B3 expression in 1B1/HEK or 1B3/HEK cells, respectively. GAPDH mRNA was used as an experimental control. The representative results obtained from three independent experiments are shown. (B and F) Western blotting was performed to examine OATP1B1 or OATP1B3 protein expression in 1B1/HEK or 1B3/HEK cells, respectively. (Asterisks indicate presumably nonglycosylated forms of each OATP1B isoform.) Na^+/K^+ ATPase was used as a loading control. The representative results that were obtained from three independent experiments are shown. (C and G) Immunocytochemistry was performed to examine OATP1B1 or OATP1B3 cell surface localization in 1B1/HEK or 1B3/HEK cells, respectively. The representative results that were obtained from three independent experiments are shown. (D and H) The OATP1B1- or OATP1B3-mediated substrate uptake activity was determined. The substrate and inhibitor for OATP1B1 experiments were E_2G (100 nM) and RIF (10 μM), respectively, and those for OATP1B3 experiments were CCK-8 (10 nM) and BSP (100 μM), respectively. Background activity level was determined by mock/HEK cells. Data represent the means ± standard deviations of the values obtained from three separate experiments, each performed in duplicate.

preincubation inhibition effects on both OATP1Bs but only at 10 μM. In contrast, preincubation with TLV and SFV did not influence OATP1B functions at all.

Examination of the long-lasting effect of preincubation inhibition of DAAs on OATP1B functions. It has been shown that preincubation inhibition effects of CsA on OATP1Bs can be maintained for several hours (15). Therefore, the long-lasting properties of the preincubation inhibition effects of SMV and ASV (1 μM) were investigated using CsA as a reference inhibitor (Fig. 4). The results showed that the residual OATP1B1 functional levels at 1 h after SMV and ASV exposure were found to be 65.1 ± 9.2% and 85.3 ± 6.1%, respectively, and that the complete recovery of OATP1B1 function was observed as early as 3 h after SMV or ASV exposure, while CsA imposed significantly prolonged inhibition on OATP1B1 function. On the other hand, SMV continuously repressed OATP1B3 function for as long as CsA did. The residual OATP1B3 activity level was 53.0 ± 12.0% at 3 h after SMV exposure. As expected, ASV lacked a preincubation inhibition effect at this concentration.

Determination of enhancing effect of DAAs' long-lasting preincubation inhibition on their overall inhibition potency against OATP1B functions. An examination was conducted to determine if the long-lasting preincubation inhibition effects of SMV and ASV augment their coincubation inhibitory level

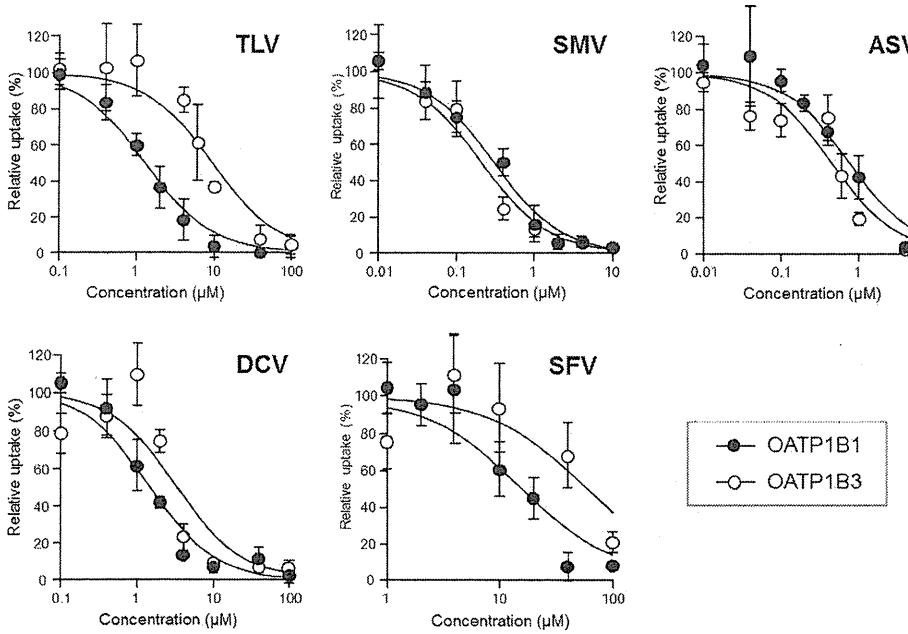

FIG 2 Interaction properties between OATP1B and DAAs determined by coincubation inhibition method. Coincubation inhibition experiments were performed in 1B1/HEK and 1B3/HEK cells using E_2G (100 nM) and CCK-8 (10 nM) for OATP1B1 and OATP1B3 substrates, respectively. TLV, SMV, ASV, DCV, and SFV were used as test inhibitors at concentrations of 0.1 to 100 μM (TLV, DCV, and SFV) and of 0.01 to 10 μM (SMV and ASV). The OATP activity level was calculated by subtracting the value obtained from mock/HEK cells from the value obtained from 1B1/HEK or 1B3/HEK cells. Data represent the means ± standard deviations of relative percentages where OATP activity level in the absence of an inhibitor (DMSO alone) was set to 100%. The values were obtained from three separate experiments, each performed in duplicate. The IC_{50} values of TLV, SMV, ASV, DCV, and SFV are summarized in Table 2.

against OATP1B functions because such effects have been identified in the case of CsA (14). Our results showed that preincubation with SMV (0.4 μM) significantly strengthened the coincubation inhibition effect (0.4 μM) on OATP1B1 activity (from 46.4 ± 2.4% to 22.3 ± 10.3%; $P < 0.05$) (Fig. 5). Preincubation with ASV (0.1 and 0.4 μM) was also found to enhance the coincubation inhibition effect on OATP1B1 activity (from 78.0 ± 2.3% to 56.1 ± 7.5% and from 50.6 ± 1.3% to 29.4 ± 7.6%, respectively; $P < 0.01$). Similar tendencies were observed at other concentrations of SMV and ASV.

Similarly, the coincubation inhibition effects of SMV at 0.1 μM on OATP1B3 function level was strengthened by preincubation with the same concentration of SMV (from 43.1 ± 6.4% to 26.5 ± 4.4%). Preincubation with ASV only marginally affected its coincubation inhibition effect on the OATP1B3 function, which was consistent with the results shown in Fig. 3 and 4.

TABLE 2 Inhibition properties of DAAs to OATP1B1/1B3 and *in vitro* evaluation of their DDI potentials through OATP1B inhibition

	OATP1B1			OATP1B3		
DAA[a]	IC_{50} (μM)	C_{max}/IC_{50}	R	IC_{50} (μM)	C_{max}/IC_{50}	R
TLV	1.36 ± 0.58	4.04	8.50	9.69 ± 3.10	0.57	2.05
SMV	0.30 ± 0.06	19.5	1.33	0.22 ± 0.07	26.6	1.45
ASV	0.79 ± 0.21	0.85	1.08	0.65 ± 0.26	1.03	1.10
DCV	1.50 ± 0.33	1.55	1.03	3.27 ± 0.57	0.71	1.01
SFV	16.5 ± 7.60	0.07	NA[b]	61.9 ± 31.6	0.02	NA[b]

[a] Anti-HCV1b efficacies of each DAA (*in vitro* 50% effective concentration value) are as follows: TLV, 354 nM (39); SMV, 8 nM (24); ASV, 1.2 nM (25); DCV, 9 pM (40); and SFV, 30 nM (41).

[b] The R value was not calculated because the C_{max}/IC_{50} value was below 0.1. NA, not available.

DISCUSSION

Our results show that all of the new DAAs examined in this study can inhibit OATP1B functions in a classical manner (coincubation inhibition) and also that some of them have distinctive long-lasting preincubation inhibitory effects on OATP1B functions. These inhibition characteristics should be seen as essential information when the clinical significance of DAA-mediated OATP1B inhibition is considered, as we have discussed herein.

Based on the criteria of R value significance (≥1.25), the values of SMV indicate that SMV creates a mild DDI risk when it is administered with OATP1B substrates. In contrast, the DDI risk potential for ASV, DCV, and SFV was found to be from very modest to negligible. These predictions are roughly consistent with the lack of literature reporting "detrimental" DDIs in association with these new agents.

Nevertheless, it has been shown that SMV administration (150 mg) leads to apparently 2- to 3-fold increases in atorvastatin (40 mg) and rosuvastatin (10 mg) exposure, respectively (Sovriad interview form, Janssen Pharmaceutical K. K., Tokyo, Japan), and that ASV administration (200 mg) results in a 1.4-fold increase in rosuvastatin (10 mg) exposure (T. Eley, Y.-H. Han, S.-P. Huang, B. He, W. Li, W. Bedford, M. Stonier, D. Gardiner, K. Sims, P. Balimane, D. Rodrigues, and R. J. Bertz, presented at the Seventh International Workshop on Clinical Pharmacology of Hepatitis Therapy, Cambridge, MA, 27 to 28 June 2012). (Please note that the clinically used dosage amounts of SMV, rosuvastatin, and atorvastatin are 100 to 150 mg once a day [QD], 5 to 40 mg QD,

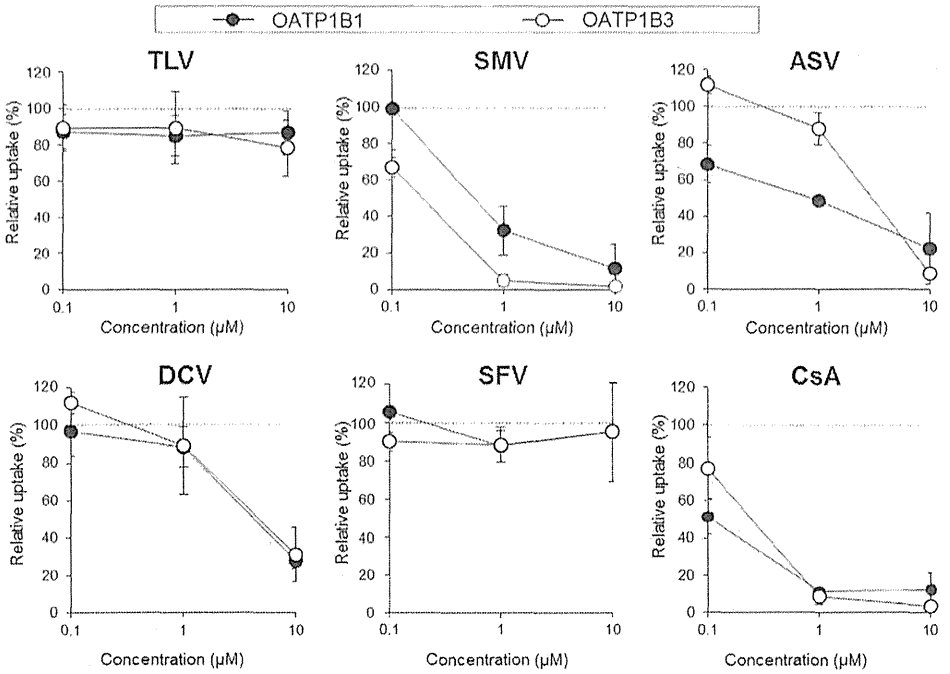

FIG 3 Preincubation inhibition effects of DAAs on OATP1B functions. E_2G (100 nM) and CCK-8 (10 nM) uptake by OATP1B1 and OATP1B3 were examined, respectively, under inhibitor-free conditions immediately after a 30-min preincubation with TLV, SMV, ASV, DCV, SFV, or CsA at 0.1, 1.0, and 10 μM (preincubation method). The OATP activity level was calculated by subtracting the value obtained from mock/HEK cells from the value obtained from 1B1/HEK or 1B3/HEK cells. Data represent the means ± standard deviations of relative percentages where the OATP activity level preincubated with DMSO alone was set to 100%. The values were obtained from three separate experiments, each performed in duplicate.

and 10 to 80 mg QD, respectively, based on their prescribing information, and that 200 mg of ASV QD or twice a day [BID] has been used in clinical trials.) Based on the results of our preincubation inhibition experiments, it can be assumed that SMV or ASV imposes long-lasting inhibition effects on OATP1B functions, in addition to their coincubation effects, in such DDIs. Preclinical data have shown that SMV and ASV accumulate significantly in rat livers (32- to 65-fold for SMV and 315-fold for ASV) (24, 25), which implies that, to the extent that they sufficiently exert preincubation inhibitory effects on OATP1B functions, unbound liver SMV or ASV concentrations might become greater than their plasma unbound concentrations. Therefore, it is reasonable to presume that the long-lasting preincubation inhibition effects of SMV or ASV play a clinically significant role in the reduction of OATP1Bs' functional levels during SMV- or ASV-containing therapy. Despite this likelihood, in order to enhance the reliability of this concept, an integrated prediction method is likely to be necessary during further investigations aimed at deter-

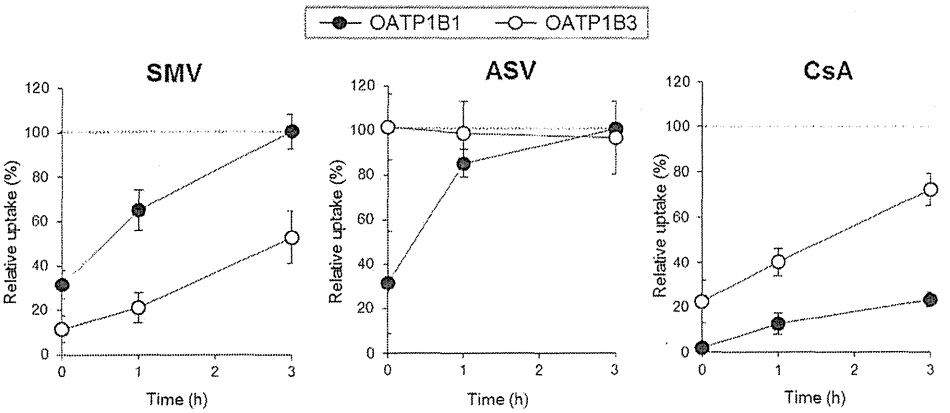

FIG 4 Long-lasting effect of preincubation inhibition of DAAs on OATP1B functions. E_2G (100 nM) and CCK-8 (10 nM) uptake by OATP1B1 and OATP1B3 was examined, respectively, under inhibitor-free conditions at 1 h, 3 h, or after just 30 min of preincubation with SMV, ASV, and CsA at 1.0 μM (long-lasting preincubation inhibition method). The OATP activity level was calculated by subtracting the value obtained from mock/HEK cells from the value obtained from 1B1/HEK or 1B3/HEK cells. Data represent the means ± standard deviations of relative percentages where the OATP activity level preincubated with DMSO alone was set to 100%. The values were obtained from three separate experiments, each performed in duplicate.

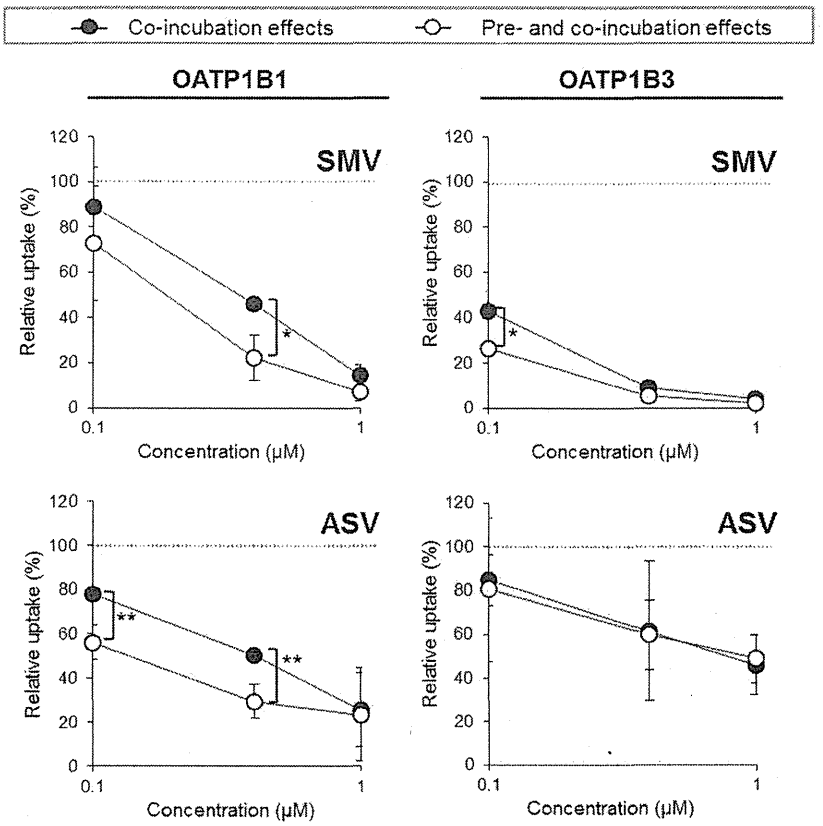

FIG 5 Enhancing effect of DAAs' long-lasting preincubation inhibition on their overall inhibition potency against OATP1B functions. E_2G (100 nM) and CCK-8 (10 nM) uptake by OATP1B1 and OATP1B3 were examined, respectively, in the presence of an inhibitor immediately after a 30-min preincubation with SMV or ASV (pre- and coincubation combination method). The inhibitor concentrations used for pre- and coincubation were equal and set at 0.1, 0.4, and 1.0 μM. The OATP activity level was calculated by subtracting the value obtained from mock/HEK cells from the value obtained from 1B1/HEK or 1B3/HEK cells. Data represent the means ± standard deviations of relative percentages where OATP activity level pre- and coincubated with DMSO alone was set to 100%. The values were obtained from three separate experiments, each performed in duplicate. Significance is indicated as follows: *, $P < 0.05$; **, $P < 0.01$.

mining the significance of OATP1B inhibition by drugs that possess both co- and preinhibition properties. Once established, such a prediction method can be expected to provide additional quantitative explanations as to why SMV and ASV affect systemic exposure of OATP1B substrates including statins.

In addition to the inhibition properties obtained in this study, it will be necessary to pay attention to the following viewpoints in order to estimate the DDI potential of DAAs *in vivo*. First, it is likely that the C_{max} and the $C_{in,max,u}$ of a DAA are highly variable among patients. For example, the C_{max} of SMV ranged from 1.8 to 13.5 μM (n = 123, HPC3003 clinical trial in Japan). This range could be further expanded as the patient population increases, partially because of the presence of rare variants in the drug-metabolizing and transporter genes (26, 27). Second, although E_2G and CCK-8 have been considered good surrogate probes for use in OATP1B inhibition studies (9, 23), the R value obtained from other OATP1B substrates may be different from the values obtained in this study, as exemplified by the report showing that the IC_{50} values of rifamycin SV toward OATP1B1-mediated E_2G and rosuvastatin uptake are 0.34 ± 0.05 and 0.05 ± 0.02 (μM), respectively (23). Finally, because various enzymes and transporters, such as CYP3A4, cooperatively determine a drug pharmacokinetic profile together with OATP1Bs, multifactor evaluation of clinical DDI likelihood is necessary in order to minimize over- or underprediction, as depicted in the recent literature (28). Therefore, DAA R values related to other gene functions should be determined and consolidated with those obtained in this study in order to create a more advanced evaluation of DDI potential of DAAs.

Taking these results together, we can suggest that SMV and (to a lesser degree) ASV have a latent potential to cause DDIs at the level of OATP1B1/1B3 even though the clinical DDI likelihood of DAAs is still open to further investigation. The possibility of this potential for DCV cannot be ruled out due to its simultaneous possession of co- and preinhibition properties, while SFV seems to be harmless to OATP1Bs.

Because chronic hepatitis C patients may often take multiple medications in addition to anti-HCV drugs, these findings will call the physician's attention to the cautions related to the DDIs associated with these DAAs (especially SMV and ASV). In addition to statins, examples of potential victim OATP substrates are repaglinide (antidiabetic), fexofenadine (antihistaminic), olmesartan and telmisartan (antihypertensives), and torsemide (diuretic) based on the literature (10, 29). Furthermore, the number of such examples can be expected to increase as new OATP1B substrate drugs are developed in the future. Therefore, even though DDIs

may not be critical factors in drug decision making, an understanding of the possible DDI risks for a DAA intended for use is nevertheless important for appropriate clinical management.

In addition, potential interactions between a DAA and an anti-human immunodeficiency virus (HIV) agent should be mentioned because ~33% of HCV patients are estimated to be coinfected with HIV in Western countries (30). According to the Sovriad interview form (Janssen Pharmaceutical K. K., Tokyo, Japan), SMV (150 mg QD) does not significantly affect rilpivirine (25 mg QD), raltegravir (400 mg QD), tenofovir (300 mg QD), or efavirenz (600 mg QD) exposure. However, although it has not yet been reported, SMV could affect lopinavir exposure, based on a report showing that its plasma concentration has been affected by the OATP1B1 function level (31, 32). On the other hand, it has been shown that efavirenz (600 mg QD) significantly reduces SMV (150 mg QD) exposure, while ritonavir (100 mg BID) increases SMV (200 mg QD) exposure in preliminary DDI tests although these are believed to be caused by alteration of SMV metabolism rate (Sovriad interview form, Janssen Pharmaceutical K. K., Tokyo, Japan). Due to the distinctive pleiotropic effects of each anti-HIV drug (or DAA) on drug-metabolizing enzymes and transporters, the *in vivo* interaction profile between an anti-HIV drug and a DAA or between any antiretroviral/DAA and its coadministered drug(s) is considerably complex. Therefore, caution related to such interactions is advisable prior to the accumulation of experimental and clinical data. A similar suggestion has been made in a recent review (33), where additional DDI information can be obtained. Considering the level of complexity, it is assumed that if antivirus-specialized clinical pharmacists could be trained, they would contribute to safer and more effective treatment for HCV/HIV-coinfected patients.

Another important issue related to the inhibition of the OATP1B function is hyperbilirubinemia. OATP1Bs play pivotal roles in development of hyperbilirubinemia because, in addition to identification of OATP1B1 and OATP1B3 as conjugated and unconjugated bilirubin transporters (11, 12), it has been shown that patients who carry biallelic inactivating mutations in both genes show rotor syndrome, which is characterized by conjugated hyperbilirubinemia (34). Clinical studies have shown that transient and benign hyperbilirubinemia without association of concomitant elevation of liver enzymes is often observed in SMV-containing regimens (35) but not in TLV-containing regimens, despite the fact that either DAA can inhibit OATP1Bs. This observation may indicate that cooperative coincubation and long-lasting preincubation inhibitory effects of SMV on both OATP1B1/1B3 functions may play a crucial role in the development of hyperbilirubinemia in SMV-containing regimens. In addition, although not fully characterized, it has been shown that SMV inhibits the bilirubin glucuronidation enzyme (UDP-glucuronosyltransferase 1A1 [UGT1A1]) and conjugated bilirubin extrusion pump (multidrug resistance protein 2 [MRP2]), while TLV does not. Therefore, the involvement of UGT1A1 and/or MRP2 inhibition in the development of SMV-mediated hyperbilirubinemia should not be ruled out even if the IC_{50} values of SMV for the bilirubin glucuronidation and MRP2 functions are higher than those for OATP1Bs (119 μM and 6.4 to 19 μM, respectively). Collectively, it is considered likely that elevation of the blood bilirubin level could reflect a functional disturbance of OATP1B1/1B3 along with UGT1A1 and/or MRP2 by SMV. Therefore, it can be speculated that extensive hyperbilirubinemia could provide a warning for SMV-caused DDI with drugs that utilize those pathways for their elimination in such patients.

Finally, the differential long-lasting preincubation effects among our DAAs should be mentioned due to their important relevant aspects in OATP1B studies. It is intriguing that SMV, ASV, and (to a lesser extent) DCV are newly listed as members of the long-lasting dual OATP1B1/1B3 inhibitor lineup, in which only CsA has been identified to date (15). In addition, it was surprising to find that, despite the outstanding similarities of their physicochemical properties (data not shown) as well as their IC_{50} values against OATP1Bs, there are significant differences in the preincubation inhibition profiles of SMV and ASV. Although the mechanisms behind their long-lasting preincubation inhibition effects remain unknown, our findings suggest that their long-lasting inhibitions against OATP1B1 and OATP1B3 do not share common cellular mechanisms and that the physicochemical property of a particular drug is unlikely to play a decisive role in its inhibition effects. Since these results may provide important insights into the clarification of inhibitory mechanisms, further mechanistic exploration using SMV and ASV can be expected to identify a key factor or process underlying long-lasting preincubation effects.

In conclusion, our results not only show that all tested DAAs are capable of inhibiting OATP1B1 and 1B3 functions but also that SMV, ASV, and DCV are newly identified, distinctive long-lasting OATP1B inhibitors. Our results also suggest that the cooperative coincubation and long-lasting preincubation inhibitory effects of SMV on OATP1B functions at least partially account for the increased exposure of statins and transient hyperbilirubinemia in SMV-containing regimens. The inhibitory effects of ASV, but not SFV, on OATP1B functions may also be clinically important, while the possibility in relation to DCV remains elusive. We expect that although such DDIs may not be the sole determinants in treatment decision making, these inhibition profiles and estimations for OATP1B-mediated DDI potentials will provide useful information that will facilitate safer and more effective anti-HCV therapy. In addition, our results point toward the need for elucidation of the detailed characteristics underlying long-lasting preincubation effects of DAAs on OATP1Bs in order to facilitate the development of an improved quantitative DDI evaluation method that takes such effects, along with other relevant factors, into consideration.

ACKNOWLEDGMENTS

We thank Yuki Suzuki and Hanae Morio (Laboratory of Pharmacology and Toxicology, Chiba University) for their technical support.

This work is funded by a Ministry of Health, Labor and Welfare Grant-in-Aid for Scientific Research (Emergency Research Project to Conquer Hepatitis), Japan.

REFERENCES

1. Shah N, Pierce T, Kowdley KV. 2013. Review of direct-acting antiviral agents for the treatment of chronic hepatitis C. Expert Opin. Investig. Drugs 22:1107–1121. http://dx.doi.org/10.1517/13543784.2013.806482.
2. Tsubota A, Furihata T, Matsumoto Y, Chiba K. 2013. Sustained and rapid virological responses in hepatitis C clinical trials. Clin. Investig. 3:1083–1093. http://dx.doi.org/10.4155/cli.13.98.
3. Burger D, Back D, Buggisch P, Buti M, Craxí A, Foster G, Klinker H, Larrey D, Nikitin I, Pol S, Puoti M, Romero-Gómez M, Wedemeyer H, Zeuzem S. 2013. Clinical management of drug-drug interactions in HCV therapy: challenges and solutions. J. Hepatol. 58:792–800. http://dx.doi.org/10.1016/j.jhep.2012.10.027.

4. Kiser JJ, Burton JR, Jr, Everson GT. 2013. Drug-drug interactions during antiviral therapy for chronic hepatitis C. Nat. Rev. Gastroenterol. Hepatol. 10:596–606. http://dx.doi.org/10.1038/nrgastro.2013.106.
5. Garg V, van Heeswijk R, Lee JE, Alves K, Nadkarni P, Luo X. 2011. Effect of telaprevir on the pharmacokinetics of cyclosporine and tacrolimus. Hepatology 54:20–27. http://dx.doi.org/10.1002/hep.24443.
6. Lee JE, van Heeswijk R, Alves K, Smith F, Garg V. 2011. Effect of the hepatitis C virus protease inhibitor telaprevir on the pharmacokinetics of amlodipine and atorvastatin. Antimicrob. Agents Chemother. 55:4569–4574. http://dx.doi.org/10.1128/AAC.00653-11.
7. Chu X, Cai X, Cui D, Tang C, Ghosal A, Chan G, Green MD, Kuo Y, Liang Y, Maciolek CM, Palamanda J, Evers R, Prueksaritanont T. 2013. In vitro assessment of drug-drug interaction potential of boceprevir associated with drug metabolizing enzymes and transporters. Drug Metab. Dispos. 41:668–681. http://dx.doi.org/10.1124/dmd.112.049668.
8. Garg V, Chandorkar G, Farmer HF, Smith F, Alves K, van Heeswijk RP. 2012. Effect of telaprevir on the pharmacokinetics of midazolam and digoxin. J. Clin. Pharmacol. 52:1566–1573. http://dx.doi.org/10.1177/0091270011419850.
9. Kunze A, Huwyler J, Camenisch G, Gutmann H. 2012. Interaction of the antiviral drug telaprevir with renal and hepatic drug transporters. Biochem. Pharmacol. 84:1096–1102. http://dx.doi.org/10.1016/j.bcp.2012.07.032.
10. Shitara Y, Maeda K, Ikejiri K, Yoshida K, Horie T, Sugiyama Y. 2013. Clinical significance of organic anion transporting polypeptides (OATPs) in drug disposition: their roles in hepatic clearance and intestinal absorption. Biopharm. Drug Dispos. 34:45–78. http://dx.doi.org/10.1002/bdd.1823.
11. Chiou WJ, de Morais SM, Kikuchi R, Voorman RL, Li X, Bow DA. 2014. In vitro OATP1B1 and OATP1B3 inhibition is associated with observations of benign clinical unconjugated hyperbilirubinemia. Xenobiotica 44:276–282. http://dx.doi.org/10.3109/00498254.2013.820006.
12. Cui Y, König J, Leier I, Buchholz U, Keppler D. 2001. Hepatic uptake of bilirubin and its conjugates by the human organic anion transporter SLC21A6. J. Biol. Chem. 276:9626–9630. http://dx.doi.org/10.1074/jbc.M004968200.
13. Shitara Y, Itoh T, Sato H, Li AP, Sugiyama Y. 2003. Inhibition of transporter-mediated hepatic uptake as a mechanism for drug-drug interaction between cerivastatin and cyclosporin A. J. Pharmacol. Exp. Ther. 304:610–616. http://dx.doi.org/10.1124/jpet.102.041921.
14. Amundsen R, Christensen H, Zabihyan B, Asberg A. 2010. Cyclosporine A, but not tacrolimus, shows relevant inhibition of organic anion-transporting protein 1B1-mediated transport of atorvastatin. Drug Metab. Dispos. 38:1499–1504. http://dx.doi.org/10.1124/dmd.110.032268.
15. Shitara Y, Takeuchi K, Nagamatsu Y, Wada S, Sugiyama Y, Horie T. 2012. Long-lasting inhibitory effects of cyclosporin A, but not tacrolimus, on OATP1B1- and OATP1B3-mediated uptake. Drug Metab. Pharmacokinet. 27:368–378. http://dx.doi.org/10.2133/dmpk.DMPK-11-RG-096.
16. Keppler D. 2014. The roles of MRP2, MRP3, OATP1B1, and OATP1B3 in conjugated hyperbilirubinemia. Drug Metab. Dispos. 42:561–565. http://dx.doi.org/10.1124/dmd.113.055772.
17. Tweedie D, Polli JW, Berglund EG, Huang SM, Zhang L, Poirier A, Chu X, Feng B, International Transporter Consortium. 2013. Transporter studies in drug development: experience to date and follow-up on decision trees from the International Transporter Consortium. Clin. Pharmacol. Ther. 94:113–125. http://dx.doi.org/10.1038/clpt.2013.77.
18. Kameyama Y, Yamashita K, Kobayashi K, Hosokawa M, Chiba K. 2005. Functional characterization of SLCO1B1 (OATP-C) variants, SLCO1B1*5, SLCO1B1*15 and SLCO1B1*15+C1007G, by using transient expression systems of HeLa and HEK293 cells. Pharmacogenet. Genomics 15:513–522. http://dx.doi.org/10.1097/01.fpc.0000170913.73780.5f.
19. Nagai M, Furihata T, Matsumoto S, Ishii S, Motohashi S, Yoshino I, Ugajin M, Miyajima A, Matsumoto S, Chiba K. 2012. Identification of a new organic anion transporting polypeptide 1B3 mRNA isoform primarily expressed in human cancerous tissues and cells. Biochem. Biophys. Res. Commun. 418:818–823. http://dx.doi.org/10.1016/j.bbrc.2012.01.115.
20. Furihata T, Satoh N, Ohishi T, Ugajin M, Kameyama Y, Morimoto K, Matsumoto S, Yamashita K, Kobayashi K, Chiba K. 2009. Functional analysis of a mutation in the SLCO1B1 gene (c.1628T>G) identified in a Japanese patient with pravastatin-induced myopathy. Pharmacogenomics J. 9:185–193. http://dx.doi.org/10.1038/tpj.2009.3.
21. Hirano M, Maeda K, Shitara Y, Sugiyama Y. 2004. Contribution of OATP2 (OATP1B1) and OATP8 (OATP1B3) to the hepatic uptake of pitavastatin in humans. J. Pharmacol. Exp. Ther. 311:139–146. http://dx.doi.org/10.1124/jpet.104.068056.
22. Hirano M, Maeda K, Shitara Y, Sugiyama Y. 2006. Drug-drug interaction between pitavastatin and various drugs via OATP1B1. Drug Metab. Dispos. 34:1229–1236. http://dx.doi.org/10.1124/dmd.106.009290.
23. Sharma P, Butters CJ, Smith V, Elsby R, Surry D. 2012. Prediction of the in vivo OATP1B1-mediated drug-drug interaction potential of an investigational drug against a range of statins. Eur. J. Pharm. Sci. 47:244–255. http://dx.doi.org/10.1016/j.ejps.2012.04.003.
24. Lin TI, Lenz O, Fanning G, Verbinnen T, Delouvroy F, Scholliers A, Vermeiren K, Rosenquist A, Edlund M, Samuelsson B, Vrang L, de Kock H, Wigerinck P, Raboisson P, Simmen K. 2009. In vitro activity and preclinical profile of TMC435350, a potent hepatitis C virus protease inhibitor. Antimicrob. Agents Chemother. 53:1377–1385. http://dx.doi.org/10.1128/AAC.01058-08.
25. McPhee F, Sheaffer AK, Friborg J, Hernandez D, Falk P, Zhai G, Levine S, Chaniewski S, Yu F, Barry D, Chen C, Lee MS, Mosure K, Sun LQ, Sinz M, Meanwell NA, Colonno RJ, Knipe J, Scola P. 2012. Preclinical profile and characterization of the hepatitis C virus NS3 protease inhibitor asunaprevir (BMS-650032). Antimicrob. Agents Chemother. 56:5387–5396. http://dx.doi.org/10.1128/AAC.01186-12.
26. O'Brien TJ, Kidd RS, Richard CA, Ha NH, Witcher P, Tran LV, Barbour A, Tuck M, McIntosh SD, Douglas JN, Harralson AF. 2013. First report of warfarin dose requirements in patients possessing the CYP2C9*12 allele. Clin. Chim. Acta 424:73–75. http://dx.doi.org/10.1016/j.cca.2013.05.008.
27. Ramsey LB, Bruun GH, Yang W, Treviño LR, Vattathil S, Scheet P, Cheng C, Rosner GL, Giacomini KM, Fan Y, Sparreboom A, Mikkelsen TS, Corydon TJ, Pui CH, Evans WE, Relling MV. 2012. Rare versus common variants in pharmacogenetics: SLCO1B1 variation and methotrexate disposition. Genome Res. 22:1–8. http://dx.doi.org/10.1101/gr.129668.111.
28. Camenisch G, Umehara K. 2012. Predicting human hepatic clearance from in vitro drug metabolism and transport data: a scientific and pharmaceutical perspective for assessing drug-drug interactions. Biopharm. Drug Dispos. 33:179–194. http://dx.doi.org/10.1002/bdd.1784.
29. Gong IY, Kim RB. 2013. Impact of genetic variation in OATP transporters to drug disposition and response. Drug Metab. Pharmacokinet. 28:4–18. http://dx.doi.org/10.2133/dmpk.DMPK-12-RV-099.
30. Sulkowski MS. 2008. Viral hepatitis and HIV coinfection. J. Hepatol. 48:353–367. http://dx.doi.org/10.1016/j.jhep.2007.11.009.
31. Kohlrausch FB, de Cássia Estrela R, Barroso PF, Suarez-Kurtz G. 2010. The impact of SLCO1B1 polymorphisms on the plasma concentration of lopinavir and ritonavir in HIV-infected men. Br. J. Clin. Pharmacol. 69:95–98. http://dx.doi.org/10.1111/j.1365-2125.2009.03551.x.
32. Hartkoorn RC, Kwan WS, Shallcross V, Chaikan A, Liptrott N, Egan D, Sora ES, James CE, Gibbons S, Bray PG, Back DJ, Khoo SH, Owen A. 2010. HIV protease inhibitors are substrates for OATP1A2, OATP1B1 and OATP1B3 and lopinavir plasma concentrations are influenced by SLCO1B1 polymorphisms. Pharmacogenet. Genomics 20:112–120. http://dx.doi.org/10.1097/FPC.0b013e328335b02d.
33. Karageorgopoulos DE, El-Sherif O, Bhagani S, Khoo SH. 2014. Drug interactions between antiretrovirals and new or emerging direct-acting antivirals in HIV/hepatitis C virus coinfection. Curr. Opin. Infect. Dis. 27:36–45. http://dx.doi.org/10.1097/QCO.0000000000000034.
34. van de Steeg E, Stránecký V, Hartmannová H, Nosková L, Hřebíček M, Wagenaar E, van Esch A, de Waart DR, Oude Elferink RP, Kenworthy KE, Sticová E, al-Edreesi M, Knisely AS, Kmoch S, Jirsa M, Schinkel AH. 2012. Complete OATP1B1 and OATP1B3 deficiency causes human Rotor syndrome by interrupting conjugated bilirubin reuptake into the liver. J. Clin. Invest. 122:519–528. http://dx.doi.org/10.1172/JCI59526.
35. Zeuzem S, Berg T, Gane E, Ferenci P, Foster GR, Fried MW, Hezode C, Hirschfield GM, Jacobson I, Nikitin I, Pockros PJ, Poordad F, Scott J, Lenz O, Peeters M, Sekar V, De Smedt G, Sinha R, Beumont-Mauviel M. 2014. Simeprevir increases rate of sustained virologic response among treatment-experienced patients with HCV genotype-1 infection: a phase IIb trial. Gastroenterology 146:430–441.e6. http://dx.doi.org/10.1053/j.gastro.2013.10.058.
36. Buti M, Agarwal K, Horsmans Y, Sievert W, Janczewska E, Zeuzem S, Nyberg L, Brown RS, Jr, Hezode C, Rizzetto M, Parana R, De Meyer S, De Masi R, Luo D, Bertelsen K, Witek J. 2014. Telaprevir twice daily is noninferior to telaprevir every 8 hours for patients with chronic hepatitis

C. Gastroenterology 146:744–753.e3. http://dx.doi.org/10.1053/j.gastro.2013.11.047.
37. Herbst DA, Reddy KR. 2013. NS5A inhibitor, daclatasvir, for the treatment of chronic hepatitis C virus infection. Expert Opin. Investig. Drugs 22:1337–1346. http://dx.doi.org/10.1517/13543784.2013.826189.
38. Lawitz EJ, Rodriguez-Torres M, Denning J, Mathias A, Mo H, Gao B, Cornpropst MT, Berrey MM, Symonds WT. 2013. All-oral therapy with nucleotide inhibitors sofosbuvir and GS-0938 for 14 days in treatment-naive genotype 1 hepatitis C (nuclear). J. Viral. Hepat. 20:699–707. http://dx.doi.org/10.1111/jvh.12091.
39. Perni RB, Almquist SJ, Byrn RA, Chandorkar G, Chaturvedi PR, Courtney LF, Decker CJ, Dinehart K, Gates CA, Harbeson SL, Heiser A, Kalkeri G, Kolaczkowski E, Lin K, Luong YP, Rao BG, Taylor WP, Thomson JA, Tung RD, Wei Y, Kwong AD, Lin C. 2006. Preclinical profile of VX-950, a potent, selective, and orally bioavailable inhibitor of hepatitis C virus NS3-4A serine protease. Antimicrob. Agents Chemother. 50:899–909. http://dx.doi.org/10.1128/AAC.50.3.899-909.2006.
40. Gao M, Nettles RE, Belema M, Snyder LB, Nguyen VN, Fridell RA, Serrano-Wu MH, Langley DR, Sun JH, O'Boyle DR, II, Lemm JA, Wang C, Knipe JO, Chien C, Colonno RJ, Grasela DM, Meanwell NA, Hamann LG. 2010. Chemical genetics strategy identifies an HCV NS5A inhibitor with a potent clinical effect. Nature 465:96–100. http://dx.doi.org/10.1038/nature08960.
41. Tong X1, Le Pogam S, Li L, Haines K, Piso K, Baronas V, Yan JM, So SS, Klumpp K, Nájera I. 2014. In vivo emergence of a novel mutant L159F/L320F in the NS5B polymerase confers low-level resistance to the HCV polymerase inhibitors mericitabine and sofosbuvir. J. Infect. Dis. 209:668–675. http://dx.doi.org/10.1093/infdis/jit562.

JVI
Journals.ASM.org

Persistent Hepatitis C Virus Infection Impairs Ribavirin Antiviral Activity through Clathrin-Mediated Trafficking of Equilibrative Nucleoside Transporter 1

Rajesh Panigrahi,[a] Partha K. Chandra,[a] Pauline Ferraris,[a] Ramazan Kurt,[a,b] Kyoungsub Song,[a] Robert F. Garry,[c] Krzysztof Reiss,[d] Imogen R. Coe,[e] Tomomi Furihata,[f] Luis A. Balart,[b] Tong Wu,[a] Srikanta Dash[a,b]

Department of Pathology and Laboratory Medicine,[a] Department of Medicine, Gastroenterology and Hepatology,[b] and Department of Microbiology and Immunology,[c] Tulane University School of Medicine, New Orleans, Louisiana, USA; Neurological Cancer Research, Stanley S. Scott Cancer Center, New Orleans, Louisiana, USA[d]; Department of Chemistry and Biology, Ryerson University, Toronto, ON, Canada[e]; Laboratory of Pharmacology and Toxicology, Graduate School of Pharmaceutical Science, Chiba University, Chiba, Japan[f]

ABSTRACT

Ribavirin (RBV) continues to be an important component of interferon-free hepatitis C treatment regimens, as RBV alone does not inhibit hepatitis C virus (HCV) replication effectively; the reason for this ineffectiveness has not been established. In this study, we investigated the RBV resistance mechanism using a persistently HCV-infected cell culture system. The antiviral activity of RBV against HCV was progressively impaired in the persistently infected culture, whereas interferon lambda 1 (IFN-λ1), a type III IFN, showed a strong antiviral response and induced viral clearance. We found that HCV replication in persistently infected cultures induces an autophagy response that impairs RBV uptake by preventing the expression of equilibrative nucleoside transporter 1 (ENT1). The Huh-7.5 cell line treated with an autophagy inducer, Torin 1, downregulated membrane expression of ENT1 and terminated RBV uptake. In contrast, the autophagy inhibitors hydroxychloroquine (HCQ), 3-methyladenine (3-MA), and bafilomycin A1 (BafA1) prevented ENT1 degradation and enhanced RBV antiviral activity. The HCV-induced autophagy response, as well as treatment with Torin 1, degrades clathrin heavy chain expression in a hepatoma cell line. Reduced expression of the clathrin heavy chain by HCV prevents ENT1 recycling to the plasma membrane and forces ENT1 to the lysosome for degradation. This study provides a potential mechanism for the impairment of RBV antiviral activity in persistently HCV-infected cell cultures and suggests that inhibition of the HCV-induced autophagy response could be used as a strategy for improving RBV antiviral activity against HCV infection.

IMPORTANCE

The results from this work will allow a review of the competing theories of antiviral therapy development in the field of HCV virology. Ribavirin (RBV) remains an important component of interferon-free hepatitis C treatment regimens. The reason why RBV alone does not inhibit HCV replication effectively has not been established. This study provides a potential mechanism for why RBV antiviral activity is impaired in persistently HCV-infected cell cultures and suggests that inhibition of the HCV-induced autophagy response could be used as a strategy to increase RBV antiviral activity against HCV infection. Therefore, it is anticipated that this work would generate a great deal of interest, not only among virologists but also among the general public.

Hepatitis C virus (HCV) is estimated to infect >185 million people worldwide (1). Infection by HCV leads to a high likelihood of chronic liver disease, which often progresses to liver cirrhosis and hepatocellular carcinoma; HCV is therefore a major public health problem. Interferon alpha (IFN-α) and ribavirin (RBV) (a guanosine analogue) have been used as standard therapy for chronic HCV infection for over a decade, with a sustained virologic response rate of 50% for genotype 1a virus. In 2011, two HCV-specific direct-acting antivirals (DAAs) targeting to NS3 protease (telaprevir and boceprevir) received FDA approval for the treatment of chronic HCV infection, along with IFN-α and RBV. Chronically HCV-infected patients treated with the triple therapy have shown significantly better viral clearance than did patients treated by a combination of IFN-α and RBV alone (2). In 2013, sofosbuvir (Sovaldi), another HCV-specific antiviral targeted to the NS5B polymerase, received FDA approval (3). These advances have allowed for more effective antiviral treatment of chronic HCV infection, permitting in some cases the use of drug combinations that do not include IFN-α. However, the new HCV DAAs are expensive, and therefore, the combination of IFN-α and RBV is still used to treat chronic HCV infection in many parts of the world.

Treatment by RBV remains an important component of combination antiviral drugs used in the treatment of chronic HCV infection. Inclusion of RBV along with other HCV antiviral drugs has been found to have significant benefits in the clearance of

Received 29 August 2014 Accepted 17 October 2014
Accepted manuscript posted online 22 October 2014
Citation Panigrahi R, Chandra PK, Ferraris P, Kurt R, Song K, Garry RF, Reiss K, Coe I, Furihata T, Balart LA, Wu T, Dash S. 2015. Persistent hepatitis C virus infection impairs ribavirin antiviral activity through clathrin-mediated trafficking of equilibrative nucleoside transporter 1. J Virol 89:626–642.
doi:10.1128/JVI.02492-14.
Editor: M. S. Diamond
Address correspondence to Srikanta Dash, sdash@tulane.edu.

doi:10.1128/JVI.02492-14

HCV infection (3). Clinical studies have shown that the inclusion of RBV in both IFN-containing and IFN-free trials prevents relapses and viral breakthrough and supports a sustained virological response (SVR) (4). In addition to HCV, RBV has been used in the treatment of a number of viruses, including respiratory syncytial virus (RSV) and Lassa virus (LASV) (5–7); RBV also inhibits the replication of other flaviviruses, such as bovine viral diarrhea virus, GB virus B, and poliovirus (a picornavirus) (8, 9). Ribavirin enters hepatocytes through nucleoside transporters, such as equilibrative nucleoside transporter 1 (ENT1), that are expressed on the plasma membrane of many cell types (10). RBV is phosphorylated by cellular kinases into RBV monophosphate (RMP), RBV diphosphate (RDP), and RBV triphosphate (RTP). The antiviral mechanism of RBV has been claimed to be at the level of inhibition of viral and cellular targets (11). Studies by a number of investigators over the years have led to the identification of a variety of mechanisms by which RBV inhibits HCV replication, including inhibition of IMP dehydrogenase (IMPDH); inhibition of mRNA capping; inhibition of viral polymerase; misincorporation of RTP by RNA polymerase, leading to chain termination; and high frequencies of mutation and error in nucleotide incorporation in the viral gene, leading to lethal mutagenesis. In addition to the mechanisms mentioned above, we recently showed that RBV directly inhibits HCV internal ribosome entry site (IRES) RNA translation at the level of polyribosome formation (12).

The reason why RBV alone does not clear HCV replication effectively has not been established. It has been reported that RBV resistance mechanisms in stable HCV replicon cell lines are due to mutations in viral RNA or to defective expression of nucleoside transporters in cells (13, 14). Other studies have found that RBV resistance in HCV-infected cell cultures is due to reduced RBV uptake and low expression levels of nucleoside transporters (15–18). The contribution of cellular factors in RBV resistance mechanisms has been described in HCV and other virus infection models (18, 19). Although the role of nucleoside transporters in antiviral resistance mechanisms has been reproduced in three separate laboratories, the mechanism(s) by which persistent HCV infection impairs RBV uptake and its antiviral activity has not been thoroughly investigated.

Previously, we reported that a combined HCV-induced endoplasmic reticulum (ER) stress and autophagy response downregulates the expression of IFN-α receptor 1, which is why HCV replication in a persistently infected cell culture is not completely inhibited by IFN-α (20, 21). In this study, we investigated virus and host cell interactions that impair RBV antiviral activity in a persistently HCV-infected cell culture system. Our results show that the sustained antiviral activity of RBV is impaired in a persistently HCV-infected cell culture. We found that HCV induces an autophagy response that impairs RBV uptake through lysosomal degradation of the ENT1 transporter. Furthermore, we show here for the first time that the cellular autophagy response due to persistent HCV replication impairs the expression of the clathrin heavy chain (CHC) molecule. The impaired expression of CHC is responsible for the reduced cell surface expression of ENT1, leading to decreased RBV uptake and impaired antiviral activity. Our results show that inhibiting the HCV-induced autophagy response restores the expression of nucleoside transporters and enhances RBV-induced HCV clearance in a persistently infected cell culture model and may lead to novel approaches to induce viral clearance.

MATERIALS AND METHODS

Cell lines, chemicals, and antibodies. The human hepatocellular carcinoma cell line Huh-7.5 was obtained from the laboratory of Charles M. Rice (Rockefeller University, New York, NY). Huh-7.5 cells were cultured in Dulbecco's modified Eagle's medium (DMEM; Life Technologies, Carlsbad, CA) supplemented with nonessential amino acids, sodium pyruvate, and 10% (vol/vol) fetal bovine serum (FBS). The *Renilla* luciferase reporter-based pJFH-ΔV3-Rluc clone used in our experiment was described previously (22). The following reagents were obtained commercially: IFN-λ1 (interleukin-29 [IL-29]) was obtained from PeproTech (Rocky Hill, NJ); Torin 1 was obtained from Selleck Chemicals (Houston, TX); RBV, hydroxychloroquine (HCQ), bafilomycin A1 (BafA1), and 3-methyladenine (3-MA) were obtained from Sigma-Aldrich (St. Louis, MO); [^{3}H]cytidine and [^{3}H]RBV were obtained from Moravek Biomedicals (Brea, CA); and plasmid pENT1-GFP was a kind gift from Imogen Coe, York University, Toronto, Canada (23). Antibodies specific for ENT1, CNT1 (Santa Cruz Biotechnology, Santa Cruz, CA), glyceraldehyde-3-phosphate dehydrogenase (GAPDH), p62, Beclin 1, clathrin heavy chain, ATG16L1, p62 (Cell Signaling Technology, Danvers, MA), HCV core protein (Thermo Fisher Scientific, Waltham, MA), and HCV NS3 (Virogen, Watertown, MA) were used.

Interferon and RBV treatment and HCV quantification. To study the mechanisms of HCV clearance by RBV, we established a stable and persistently HCV-infected cell culture system with Huh-7.5 cells that releases infectious virus particles and enables quantification of HCV replication by the measurement of *Renilla* luciferase, Western blotting, and immunostaining (20). RBV treatment of HCV-infected cultures was performed in six-well tissue culture plates (Costar; Corning, Tewksbury, MA) in triplicate. Huh-7.5 cells (2×10^4 cells) were plated into six-well tissue culture plates, and the next day, they were infected overnight with cell culture-grown JFH-ΔV3-Rluc recombinant HCV at a multiplicity of infection (MOI) of 0.1. The following day, the infected Huh-7.5 cells are washed twice with phosphate-buffered saline (PBS) and then cultured in DMEM containing 10% FBS. RBV and IFN-λ1 treatment was then performed at 3 days postinfection. For the first plate, the upper three wells were mock treated, and the bottom three wells were treated with 5 μg/ml of RBV. For the second plate, the upper three wells were treated with 20 μg/ml of RBV, and the bottom three wells were treated with 25 μg/ml of IFN-λ1. Both untreated and treated cultures were split at 3-day intervals at a 1:3 ratio. During passaging, one-third of the cells were seeded for a second round of treatment (T2). The remaining two-thirds of cells were used to measure the level of HCV replication by *Renilla* luciferase assays, Western blotting for HCV core protein, and immunocytochemistry for HCV core protein. The *Renilla* luciferase activity of the protein lysate was measured by using a commercially available luciferase assay kit (Promega, Madison, WI). Twenty micrograms of protein lysates was used to measure the expression level of HCV core protein by Western blotting using a standard protocol established in our laboratory (20). Two hundred microliters of infected Huh-7.5 cells (1×10^5 cells/ml) was immobilized on glass slides by the cytospin method. Expression of HCV core protein was measured by immunostaining using a standard protocol established in our laboratory (20). The number of HCV core-positive cells in 10 different high-power fields (magnification, ×40) was measured in RBV-treated and untreated HCV-infected cultures.

RBV cytotoxicity. The cellular toxicity of RBV in uninfected and HCV-infected Huh-7.5 cell cultures was quantified by 3-(4,5-dimethylthiazol-2-yl)-2,5-diphenyltetrazolium bromide (MTT) assays. In brief, cells were seeded onto 24-well plates at a density of 2×10^4 cells/well in Dulbecco's modified Eagle's medium with 10% fetal bovine serum overnight. The next day, cells were treated with increasing concentrations of RBV (10 to 60 μg/ml). After 48 h of incubation, the cells were washed twice with PBS, 100 μl of MTT solution along with 900 μl of growth medium were added to each well, and the cells were incubated at 37°C for 3 h. The cells were then washed twice in PBS and then solubilized with 1 ml of MTT solubilization buffer (anhydrous isopropanol containing 10%

Triton X-100–0.1 N HCl) for 5 min. Absorbance was measured with a spectrophotometer (DU-530; Beckman Coulter, Brea, CA) at a wavelength of 570 nm. The concentration of RBV that permits the highest cell viability was determined.

RBV uptake. RBV uptake into persistently HCV-infected cells was measured by using a previously described protocol (20). HCV-infected Huh-7.5 cells were harvested by trypsin-EDTA treatment and washed twice with DMEM supplemented with 10% FBS. A total of 1×10^6 infected cells were suspended in 1 ml of growth medium in sterile polystyrene, round-bottom tubes with a cap. The RBV uptake assay was carried out with 100 μl of DMEM containing either 5 μM ^{3}H-labeled RBV or [^{3}H]cytidine (as a control) at 37°C with continuous shaking. After 30 min of incubation, cells were washed with 1 ml of ice-cold PBS for 5 min to stop the reaction. After this step, cells were washed twice with 1 ml of ice-cold PBS. Cell pellets were treated with 100 μl of lysis buffer (10 mmol/liter Tris-HCl [pH 8.0], 10 mmol/liter NaCl, 1.5 mmol/liter $MgCl_2$, and 0.1% [vol/vol] NP-40). Forty microliters of the soluble protein lysate was mixed with 1 ml of scintillation fluid, and radioactivity was measured by using a scintillation analyzer (PerkinElmer, Walton, MA). Uptake values were expressed as counts per minute. The data were normalized to account for cell numbers per well.

Measurement of the autophagy response in HCV-infected cells. The autophagy response in HCV-infected Huh-7.5 cells was determined by measuring the expression of p62 by immunostaining and Western blot analysis. Immunostaining and Western blotting for p62 expression were performed by using a protocol identical to the one described above (20). A flow cytometry-based quantitative analysis was employed to determine whether the loss of p62 expression due to an autophagy response correlates with increased HCV core expression in the infected culture. The experiment was performed in triplicate. For this purpose, Huh-7.5 cells in three 10-cm tissue culture dishes were infected with HCV, and the expression levels of p62 and core protein in the infected culture were measured at 0, 3, 6, 9, and 12 days. Both uninfected and HCV-infected Huh-7.5 cells were split at 3-day intervals at a 1:3 ratio. One-third of the cells were seeded into 10-cm tissue culture dishes for subsequent analysis. The remaining two-thirds of cells were utilized to measure the expression levels of p62 and HCV core after immunofluorescence staining. Briefly, cells were fixed for 10 min with 2% (wt/vol) paraformaldehyde in PBS and then permeabilized for 15 min by using ice-cold methanol. After this step, cells were divided into two parts: one half of the cell suspension was used for immunofluorescence staining to measure HCV core expression, and the other half was used to measure p62 expression. For the detection of p62 expression, infected cells were incubated with a rabbit monoclonal antibody tagged with Alexa Fluor 488 (1:100 dilution) for 60 min. After this step, cells were washed in growth medium twice, and the pellet was suspended in 1 ml of PBS and directly analyzed by flow analysis. For the detection of HCV core, cells were first incubated with a mouse monoclonal antibody (1:200) for 60 min. After two washings with growth medium, cells were incubated with goat anti-mouse Alexa Fluor 488-conjugated secondary antibody (1:500) (Life Technologies, Carlsbad, CA) for 1 h at 37°C. Following this step, the cells were washed twice in growth medium and then suspended in 1 ml of PBS. The presence of HCV core in uninfected and HCV-infected Huh-7.5 cells was detected separately by using a flow cytometer (Beckman Coulter, Pasadena, CA). The percentage of cells showing positive expression of p62 and HCV core in the infected culture at 0, 3, 6, 9, and 12 days postinfection was recorded.

The presence of the autophagosomal marker LC3-II as determined by Western blotting reflects autophagic activity in mammalian cells. Measurement of the LC3 proteins assessed the induction of the autophagy response in the HCV-infected culture. Acridine orange staining was used to visualize the formation of autophagolysosomes in infected Huh-7.5 cells by fluorescence microscopy. Infected Huh-7.5 cells in a six-well tissue culture plate were incubated with 5 μg/ml acridine orange for 15 min. Cells were washed and examined under a fluorescence microscope. Acridine orange dye present in the acidic environment due to induction of autophagy appears orange, whereas dye present in a nonacidic environment appears green. The color change from green to orange was monitored under an Olympus microscope (magnification, ×40). Autophagy is a lysosomal degradation pathway for cytoplasmic material. Electron microscopy was utilized to confirm the autophagy response in the HCV-infected culture by using a standard protocol previously described (20).

Sorting of RBV-sensitive and RBV-resistant HCV-infected cells by flow cytometry. Huh-7.5 cells cultured in six 10-cm dishes were infected with HCV at an MOI of 0.1. On day 12, three plates were treated with RBV at 20 μg/ml, and the remaining three plates were untreated. After two rounds of RBV (20 μg/ml) treatment, cells were harvested and stained for intracellular core, and HCV-positive and HCV-negative cells were then sorted by flow cytometry. Intracellular core staining was performed by using the following protocol. A total of 1×10^7 HCV-infected cells were fixed for 10 min with 2% (wt/vol) paraformaldehyde in PBS. After this step, cells were washed once with DMEM containing 5% (vol/vol) FBS and then treated with 1 ml of 1× fluorescence-activated cell sorting (FACS) permeabilizing solution (0.5% [wt/vol] saponin in PBS) at room temperature. Cells were then incubated with a monoclonal antibody to HCV core protein (1:200 dilution) for 60 min at room temperature. The cells were then washed twice with DMEM containing 5% (vol/vol) FBS and incubated with Alexa Fluor 488-conjugated goat anti-mouse secondary antibody (1:500) (Life Technologies, Carlsbad, CA) for 1 h at 37°C. After this step, the cells were washed twice in PBS and then resuspended in 1 ml of PBS. RBV-sensitive (HCV core-negative) and RBV-resistant (core-positive) cells were separated by flow sorting with a FACSAria system (BD Bioscience, San Jose, CA). Sorted cells were lysed, and expression levels of ENT1 and clathrin were measured by Western blotting.

Real-time RT-qPCR. Total RNA was isolated from uninfected and HCV-infected Huh-7.5 cells by using the guanidinium thiocyanate (GITC) method. HCV quantification was carried out by using a reverse transcription-quantitative PCR (RT-qPCR) assay described previously (21). Briefly, 1 μg of total cellular RNA was used to amplify the 5′ untranslated region (UTR) of the HCV genome by using sense primer 5′-TCTTCACGCAGAAAGCGTCTA-3′ (positions 60 to 80) (HCV/S) and antisense primer 5′-CGGTTCCGCAGACCACTATG-3′ (positions 157 to 138) (HCV/AS). The probe (5′-56-FAM-TGAGTGTCG-ZEN-TGCAGCCTCCAGGA-3IBκFQ-3′), labeled at the 5′ ends with a 6-carboxyfluorescein (FAM) fluorophore reporter molecule and ZEN-Iowa Black FQ (IBFQ) double quenchers, was used to reduce the background and increase the signal (Integrated DNA Technologies Inc.). Briefly, the RT reaction of HCV RNA was carried out by using a standard method established in our laboratory. An aliquot of 1 μg of total RNA was incubated with 500 ng of antisense primer and incubated at 65°C for 10 min, followed by immediate chilling on ice. This template primer mix was subsequently incubated with a solution containing 10 units of avian myeloblastosis virus (AMV) reverse transcriptase (Promega, Madison, WI, USA), 1.5 mM $MgCl_2$, 1 mM deoxynucleoside triphosphate (dNTP) mix, and 40 units RNaseOut (Invitrogen, Carlsbad, CA, USA) in a 20-μl total reaction mixture volume for 90 min at 42°C. An identical reaction without the addition of RT enzyme was used as the control. After the cDNA synthesis step, a qPCR assay was carried out with a 20-μl solution containing 10 μl of iQ Supermix (Bio-Rad Laboratories Inc., Hercules, CA), 0.25 μM each primer and probe, and 4 μl of the cDNA product obtained from the RT reaction. Each reaction was run in triplicate. Amplification was carried out by using a standard program, with the first cycle at 48°C for 30 min and 95°C for 10 min, followed by 45 additional cycles. Each PCR cycle included a denaturation step at 95°C for 15 s and then an annealing-and-extension step at 60°C for 1 min. The cDNA standards were used starting at 1×10^9 copies of virus and decreasing in 10-fold serial dilutions for HCV copy number determination. Amplification, data acquisition, and analysis were carried out by using a CFX96 real-time instrument with CFX Manager software (Bio-Rad Laboratories Inc.).

The mRNA levels of ENT1, CNT1, CHC, and glyceraldehyde-3-phosphate dehydrogenase (GAPDH) (as an internal control) were quantified

by using RT-qPCR. The expression level of each mRNA was compared with the GAPDH mRNA level by using the comparative threshold cycle ($\Delta\Delta C_T$) method. The reverse transcription reaction for each mRNA was carried out by using standard methods as described above except for the gene-specific antisense primer. The qPCR assay was carried out in a 20-μl solution containing 10 μl of iQ Supermix (Bio-Rad Laboratories Inc.), 0.25 μM each primer, and 4 μl of cDNA product obtained from the RT reaction. Each reaction was run in triplicate. Amplification was carried out by using a standard program, with the first cycle at 50°C for 2 min and 95°C for 8 min, followed by 45 additional cycles. Each PCR cycle included a denaturation step at 95°C for 20 s and then an annealing-and-extension step at 60°C for 1 min. The nucleotide sequences of oligonucleotide primers for ENT1 mRNA (sense primer 5′-CTCTCAGCCCACCAATGAAA G-3′ and antisense primer 5′-CTCAACAGTCACGGCTGGAA-3′), CNT1 mRNA (sense primer 5′-CCTCACCTGTGTGGTCCTCA-3′ and antisense primer 5′-AGACCCCTCTTAAACCAGAGC-3′), and CHC mRNA (sense primer 5′-ATGGTGCTCTTTGTTCCTGAATG-3′ and antisense primer 5′-CTAGTGTGTTGCTCACTTCATGTGTAA-3′) were derived from previous reports (24). Amplification, data acquisition, and analysis were performed on the CFX96 real-time instrument using CFX manager software (Bio-Rad, Hercules, CA).

Colocalization of HCV, clathrin, and ENT1 expression as determined by fluorescence microscopy. The effect of HCV replication on the expression of clathrin and ENT1 was confirmed by colocalization studies. Uninfected and HCV-infected Huh-7.5 cells (1×10^6) were harvested by trypsin-EDTA treatment and washed twice in DMEM containing 5% (vol/vol) FBS in 1.5-ml tubes. The cells were fixed for 10 min with 2% (wt/vol) paraformaldehyde in PBS, washed once with DMEM containing 5% (vol/vol) FBS, and then treated with 1 ml of 1× FACS permeabilizing solution in PBS at room temperature. The cells were incubated with a rabbit polyclonal antibody at a dilution of 1:400 for the detection of the clathrin heavy chain (Cell Signaling, Danvers, MA) and a mouse monoclonal antibody against HCV core (1:200 dilution) (Thermo Scientific, Waltham, MA) for 1 h with gentle shaking at room temperature. After this step, the cells were then washed once with DMEM containing 5% (vol/vol) FBS and incubated with Alexa Fluor 488 (green)-labeled goat anti-rabbit (Life Technologies, Carlsbad, CA) secondary antibody specific for clathrin heavy chain detection and Texas Red (red)-conjugated goat anti-mouse secondary antibody for the detection of HCV core at a dilution of 1:500 (Life Technologies, Carlsbad, CA), together, at room temperature with shaking. After 30 min of incubation, cells were washed twice with DMEM containing 5% (vol/vol) FBS, and an aliquot of the cell suspension was examined for clathrin heavy chain and HCV core expression by fluorescence microscopy using green and red channels. Individual fluorescence images were captured and processed by using a Leica DFC345 FX fluorescence microscope with a ×60 magnification, and composite images were generated by using Metamorph software. The effect of HCV infection on ENT1-green fluorescent protein (GFP) expression was examined by confocal microscopy. Uninfected and HCV-infected Huh-7.5 cells in six-well plates (1×10^5 cells/well) were transfected with 0.5 μg of the ENT1-GFP plasmid by using TurboFect (Thermo Scientific, Waltham, MA). After 48 h, cells were immunostained for HCV core by using a procedure identical to the one described above. After immunostaining, an aliquot of the cell suspension was examined for HCV core and ENT1-GFP expression by confocal microscopy at a ×100 magnification (Olympus, Shinjuku, Tokyo, Japan).

siRNA transfection. Small interfering RNA (siRNA) oligonucleotides specific for CHC and ATG16L1 were obtained from Qiagen (MD, USA). All-Star siRNA, obtained from Qiagen, was used as a negative control. Sequences of the siRNAs targeting the indicated proteins are as follows: 5′-TAATCCAATTCGAAGACCAAT-3′ for CHC and 5′-CAGA ACTTGATTGTAAATAAA-3′ for ATG16L1. Huh-7.5 cells were seeded into a 6-well plate (1×10^5 cells/well). After 24 h, the cells were transfected with 25 pmol and 50 pmol siRNA per well by using Lipofectamine 2000 (Invitrogen, Carlsbad, CA) according to the manufacturer's instructions. After 48 h, silencing efficacy was determined by Western blotting using antibodies specific to clathrin and ATG16L1 (Cell Signaling, Danvers, MA).

Statistical analysis. All measurements were made at least in triplicate. All results were expressed as means ± standard deviations. Comparison between two groups was performed with Student's *t* test. To compare means within groups, we performed one-factor analysis of variance (ANOVA) using Graph Pad Prism software. We assumed that all measurements have normal probability distributions, which is expected for these types of data. The *P* value for the ANOVA was significant when the *P* value was <0.05.

RESULTS

Ribavirin antiviral activity is impaired in persistently HCV-infected cells. A persistently HCV-infected cell culture model was developed with Huh-7.5 cells to study the mechanisms of RBV resistance. Huh-7.5 cells were infected with JFH1-ΔV3-Rluc chimera virus at a multiplicity of infection (MOI) of 0.1 for 72 h, and the infected culture was then passaged every 3 days by splitting at a ratio of 1:3. Replication of HCV in the infected culture was confirmed by *Renilla* luciferase expression (Fig. 1A). *Renilla* luciferase readings of infectivity assay results were recorded in triplicate. Western blot analysis was performed to verify that HCV-infected Huh-7.5 cells expressed high levels of core and NS3 proteins (Fig. 1B). The degree of HCV replication and the spread of the infected culture at different time intervals were assessed by performing immunostaining for viral core protein expression (Fig. 1C). A quantitative assessment of HCV core-positive cells in the infected culture was performed by counting brown-stained cells in 10 different fields at a ×40 magnification. The results showed that the number of core-positive cells in the infected culture increased during the 12-day assessment period (Fig. 1D). Quantification of HCV core-positive cells by flow cytometry revealed that 60% to 70% of cells were persistently infected with HCV on day 12 (data not shown). These results indicate persistent HCV replication in the infected Huh-7.5 cell culture. The HCV-infected Huh-7.5 cell culture system was therefore utilized to investigate the RBV antiviral resistance mechanism.

The viabilities of uninfected and HCV-infected cells were >90% at 24 h when treated with increasing concentrations of RBV (10 to 60 μg/ml). Huh-7.5 cells were seeded into 6-well tissue culture plates with HCV at an MOI of 0.1; on day 3, the cells were treated with two different concentrations of RBV (5 μg/ml and 20 μg/ml) and with IFN-λ1 (IL-29) (25 μg/ml) for over 12 days. *Renilla* luciferase values of untreated cultures increased gradually from T0 to T3 (days 3 to 12), indicating active HCV replication in the infected culture (Fig. 2A). Infected cells treated with IFN-λ1 showed a sustained and significant decrease in *Renilla* luciferase activity after the third treatment. However, RBV antiviral activity was found to be impaired in the HCV-infected cell culture.

The relative antiviral potencies of RBV and IFN-λ1 were compared based on the percent inhibition of the luciferase reading over the course of three treatments (Fig. 2B). The antiviral activity of RBV, applied at a concentration of 20 μg/ml, increased to 40% by T0 (3 days) and to ~50% by T1 (6 days) and then decreased to 20% by the third treatment (T3) (12 days). The *Renilla* luciferase results for the RBV and IFN-λ1 treatments were confirmed by measuring HCV core protein expression by immunohistochemical staining. The number of HCV core-expressing cells in the untreated and RBV-treated cultures progressively increased, com-

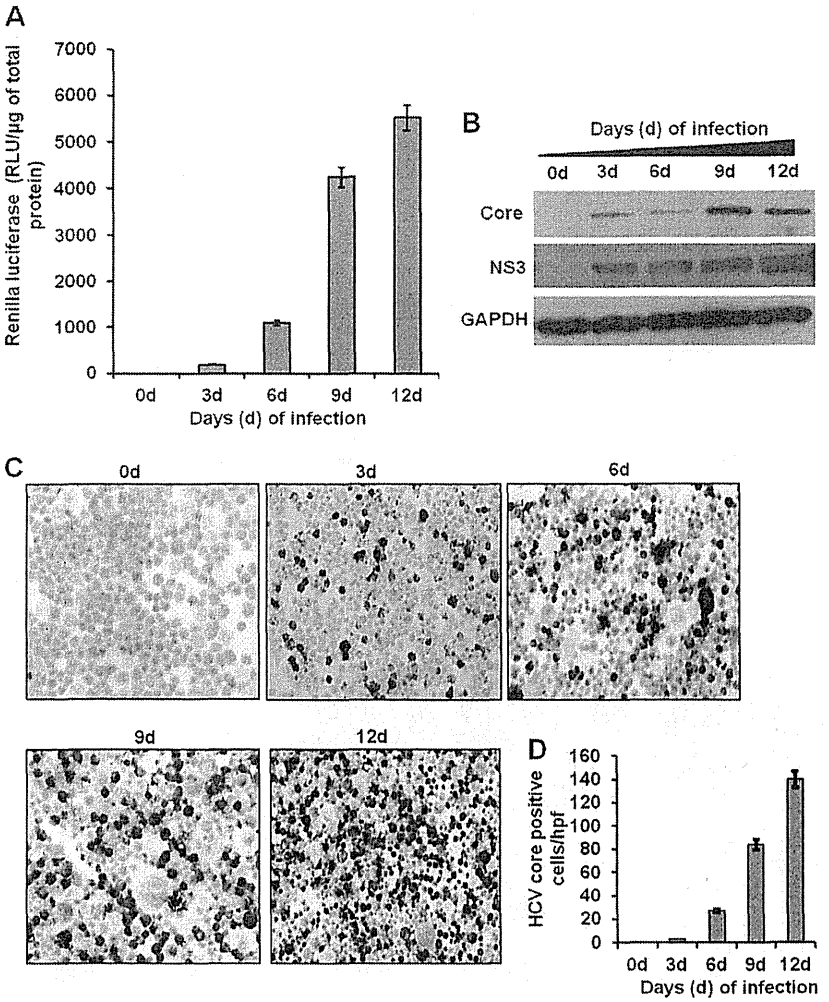

FIG 1 Persistent HCV replication in Huh-7.5 cells. Huh-7.5 cells were infected overnight with JFH-ΔV3-Rluc virus at an MOI of 0.1 and passaged at 3-day intervals. (A) *Renilla* luciferase activity of infected cell lysates. RLU, relative light units. (B) HCV core and NS3 protein levels in infected cells measured by Western blotting. GAPDH served as a loading control. (C) Immunocytochemical staining of uninfected (0 days) and infected (3 to 12 days) Huh-7.5 cells using a monoclonal antibody specific for HCV core protein. (D) Quantitative assessment of HCV core protein expression in infected cultures made by counting positive cells in 10 different high-power fields (hpf) at a magnification of ×40.

pared with the numbers in the IFN-λ1-treated culture (Fig. 2C). These results are consistent with our previous reports indicating that IFN-λ1 induces HCV clearance (20). The numbers of HCV core-positive cells in each treatment group were counted, and the results were compared for statistical significance (Fig. 2D). The core expression results are in agreement with *Renilla* luciferase readings, which indicate impaired RBV antiviral activity in HCV-infected cells. These results were further confirmed by measuring HCV RNA levels by RT-qPCR using primer sets targeted to the 5′ UTR (Fig. 2E). To rule out the possibility that the RBV used in our antiviral assay may have lost its antiviral activity, the same preparation was used against the replicon cell line R4-GFP (a stable subgenomic replicon cell line), on which it showed a strong inhibitory effect (data not shown). As demonstrated previously by our group (12), RBV at a concentration of 200 μg/ml does not produce any statistically significant decrease in cell viability in HCV-infected cultured cells, indicating that the observed pattern of RBV antiviral activity was not due to differential cytotoxicity of RBV (data not shown).

HCV infection impairs RBV uptake and expression of RBV transporters. Nucleoside transporters are involved in the uptake of RBV by hepatocytes, and decreased RBV uptake has been reported to be a reason for impaired RBV activity against HCV infection (15). We compared RBV uptake in an untreated HCV-infected culture at 3-day intervals for up to 12 days in triplicate experiments. The results of the assays indicate that RBV uptake in HCV-infected cells decreases in a time-dependent manner, with the maximum decrease occurring on day 12 (Fig. 3A). Ribavirin is transported into hepatocytes via nucleoside transporters (ENT1 and CNT1) (10). We assessed whether the mechanism of the reduction of uptake RBV by the infected culture could be related to differences in ENT1 and CNT1 mRNA levels. Total RNA was isolated from HCV-infected cultures on days 0, 3, and 12, and CNT1 and ENT1 mRNA levels were measured by real-time RT-qPCR.

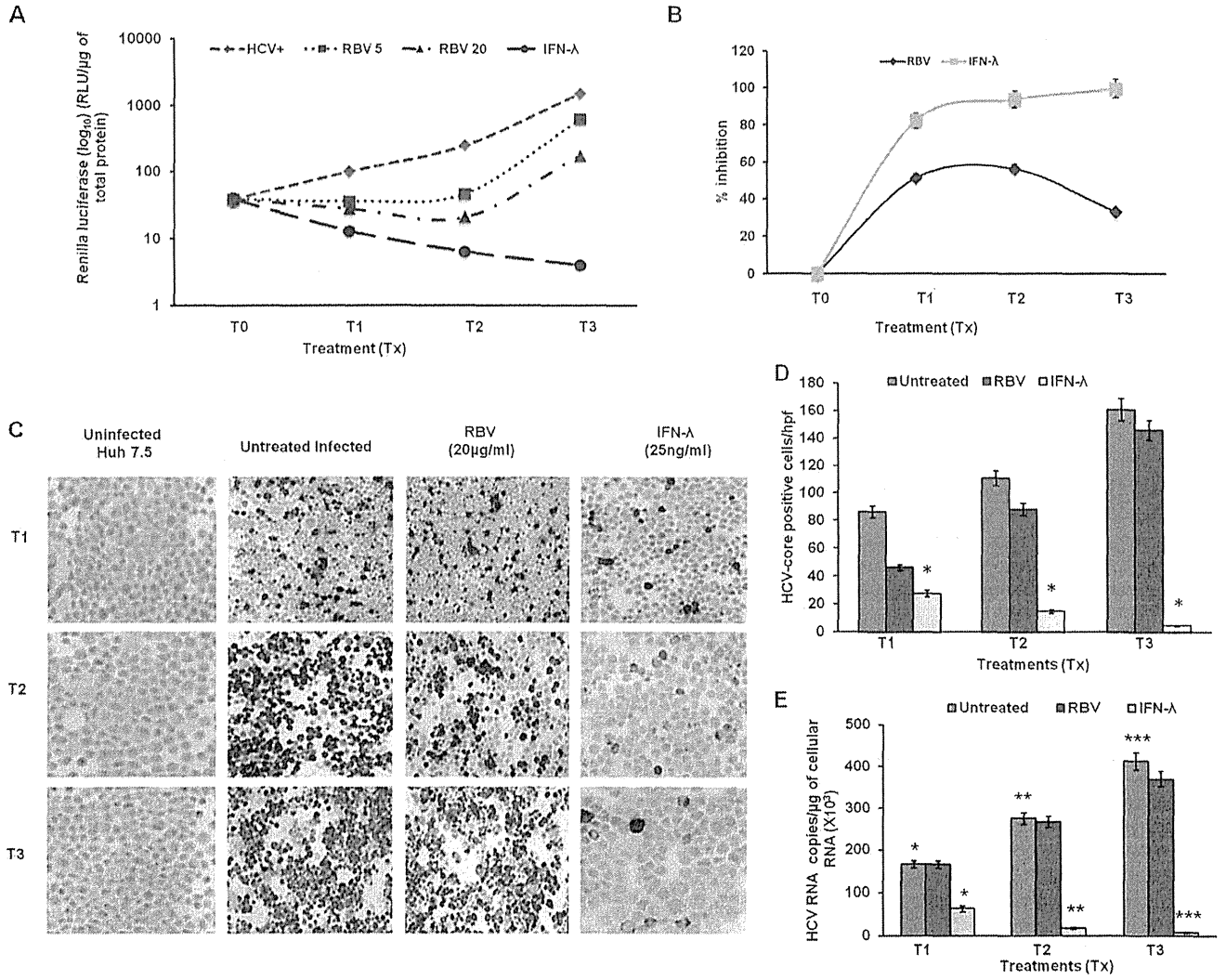

FIG 2 RBV antiviral activity is impaired in HCV-infected Huh-7.5 cells. HCV-infected Huh-7.5 cells on day 3 were continuously treated with either RBV (5 μg/ml and 20 μg/ml) or IFN-λ1 (25 ng/ml). (A) Inhibitory effect of RBV and IFN-λ1 assessed by measurement of *Renilla* luciferase activity produced by JFH-ΔV3-Rluc virus. (B) Percent inhibition of HCV replication by RBV (20 μg/ml) and IFN-λ1 (25 ng/ml). (C) HCV core protein (brown) detected by immunohistochemistry in infected T1 (6 days), T2 (9 days), and T3 (12 days) cultures. (D) HCV core-positive cells were counted in 10 different high-power fields (hpf) at a ×40 magnification, and mean cell numbers between RBV-treated and IFN-λ1-treated cultures were compared (*, $P < 0.05$). (E) HCV RNA levels of HCV-infected Huh-7.5 cells treated with RBV and IFN-λ1 (*, $P < 0.05$; ** $P < 0.001$; ***, $P < 0.0001$).

The results of this assay indicate that HCV infection actually induced the expression of ENT1 and CNT1 mRNAs (Fig. 3B). Next, we verified whether the impaired uptake of RBV is related to ENT1 and CNT1 protein degradation. The ENT1 and CNT1 expression levels in HCV-infected cultures with and without RBV treatment were examined by Western blotting. We found that ENT1 and CNT1 protein levels decreased in HCV-infected untreated cultures from days 3 to 12, compared with levels in uninfected Huh-7.5 cultures (Fig. 3C). In this assay, we found that decreased expression levels of ENT1 and CNT1 correlated with the expression of HCV NS3 protein in the infected culture. We also noticed that the decrease in the expression level of ENT1 in the infected culture was greater than that of CNT1. As ENT1 is the primary nucleoside transporter relevant to RBV uptake by hepatocytes, these results provide an explanation for why RBV antiviral activity progressively decreases in HCV-infected cultures (10).

We next compared ENT1 expression levels in RBV-treated HCV-infected and uninfected Huh-7.5 cell cultures over the course of three RBV treatments (T1, T2, and T3). The expression of ENT1 was very similar to that in the HCV-infected culture, indicating that RBV treatment has no effect on ENT1 expression in either HCV-infected or uninfected cultures (Fig. 3D). We found that the decrease in ENT1 expression was correlated with an increase in HCV core protein levels in the RBV-treated culture. This effect appears to be specific to HCV infection, as Western blot analysis showed that RBV treatment has no effect on the expression of ENT1 in uninfected Huh-7.5 cells (Fig. 3E). Because IFN-λ1 effectively inhibits HCV in infected cultures, we verified whether ENT1 expression was restored in these cultures. Indeed, levels of ENT1 expression were gradually restored in the IFN-λ1-treated (T1, T2, and T3) cultures (Fig. 3F). The expression of HCV core protein was reduced due to IFN-λ1 treat-

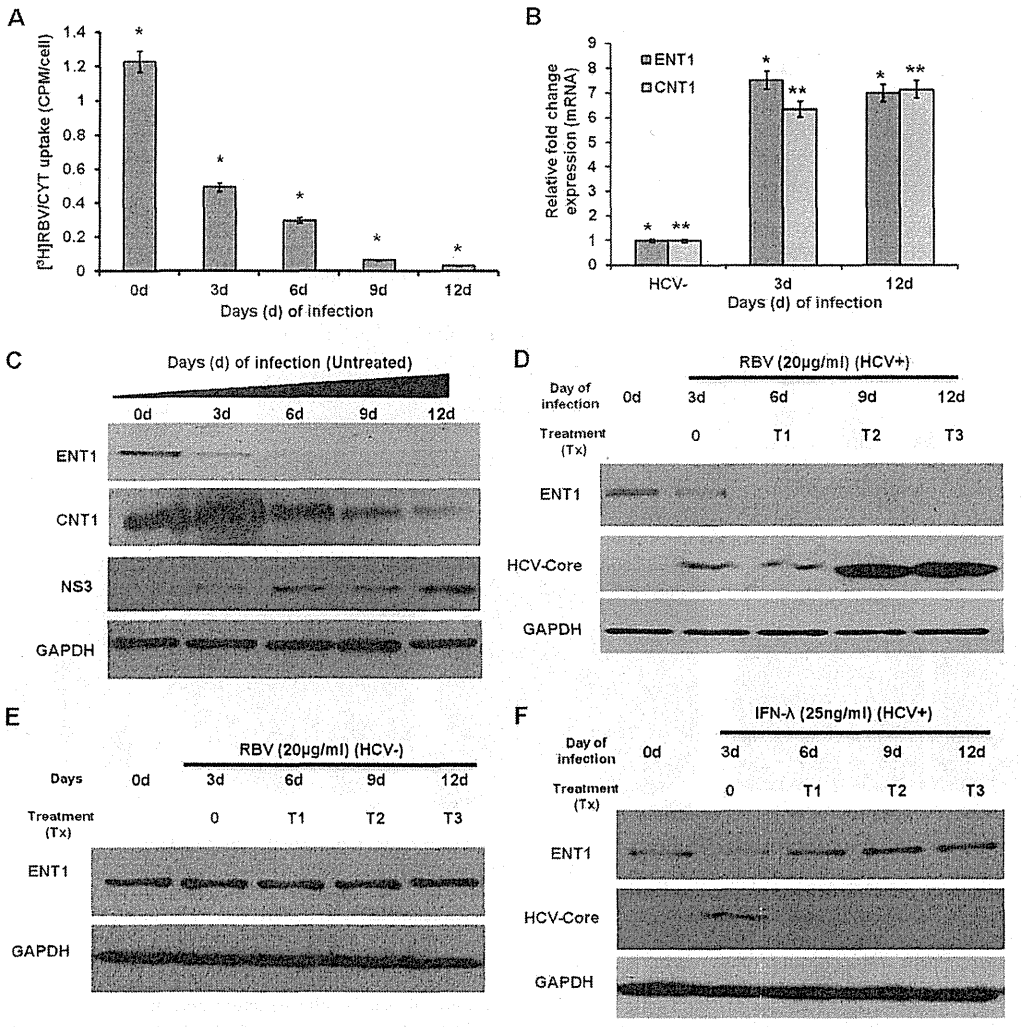

FIG 3 RBV uptake in HCV-infected cultures is impaired due to reduced expression of the RBV transporter (ENT1). RBV uptake and expression of nucleoside transporters were compared up to 12 days in HCV-infected Huh-7.5 cells. (A) [^{3}H]RBV and [^{3}H]cytidine (CYT) uptake in HCV-infected Huh-7.5 cells (*, $P < 0.05$). CPM, counts per minute. (B) Real-time RT-qPCR for ENT1 and CNT1 mRNA levels in HCV-infected Huh-7.5 cells. Total RNA was isolated from uninfected and infected Huh-7.5 cells (3 days and 12 days), and the relative levels of ENT1, CNT1, and GAPDH mRNAs were assessed by real-time RT-qPCR (*, $P < 0.05$; **, $P < 0.001$). (C) ENT1 and CNT1 protein levels in untreated HCV-infected Huh-7.5 cells measured by Western blotting. The GAPDH level was measured as a loading control. HCV NS3 levels of untreated cells are shown for comparison. (D) Western blot analysis of ENT1, HCV core, and GAPDH in HCV-infected cells treated with RBV (20 μg/ml). (E) Western blot analysis of ENT1 and GAPDH levels in uninfected Huh-7.5 cells treated with RBV (20 μg/ml). (F) Western blot analysis of ENT1, HCV core, and GAPDH in HCV-infected cells treated with IFN-λ1 (25 ng/ml).

ment, thus confirming that ENT1 expression is regulated by HCV replication. The GAPDH levels remained at comparable levels in all experiments, indicating that comparable amounts of protein were loaded into each well for Western blot analysis. Taken together, all of these results indicate that HCV infection selectively degrades ENT1 and CNT1 protein levels without altering mRNA levels.

The HCV-induced autophagy response degrades ENT1 and impairs RBV uptake. Autophagy is a key cellular lysosomal degradation process that has been implicated in the establishment of persistent HCV infection (25). Infection by HCV has been shown to induce both ER stress and an autophagy response in hepatocytes (20). Induction of the cellular autophagy response in HCV-infected Huh-7.5 cell cultures was confirmed by a number of assays. Microtubule-associated protein (LC3) and p62 are the two key components in the formation of autophagosomes (26). During autophagy, the cytoplasmic form of LC3 (LC3-I) (18 kDa) is recruited to the autophagosome, where LC3-II (16 kDa) is generated by site-specific proteolysis and lipidation near the C terminus (27); p62, on the other hand, binds LC3 and recruits proteins to autophagosomes for degradation. Thus, increased LC3-II and decreased p62 levels indicate autophagic activity, whereas p62 accumulation indicates insufficient autophagy.

The basal level of autophagy is inefficient in human hepatocellular carcinoma cells (28). Immunostaining of HCV-infected Huh-7.5 cells shows a decrease in the expression level of the p62 protein over 0 to 12 days, which is an indication of autophagy induction (Fig. 4A). Flow analysis shows that the expression level of p62 in the infected culture decreased over 12 days (Fig. 4B). A flow cytometry-based quantitative analysis demonstrated that

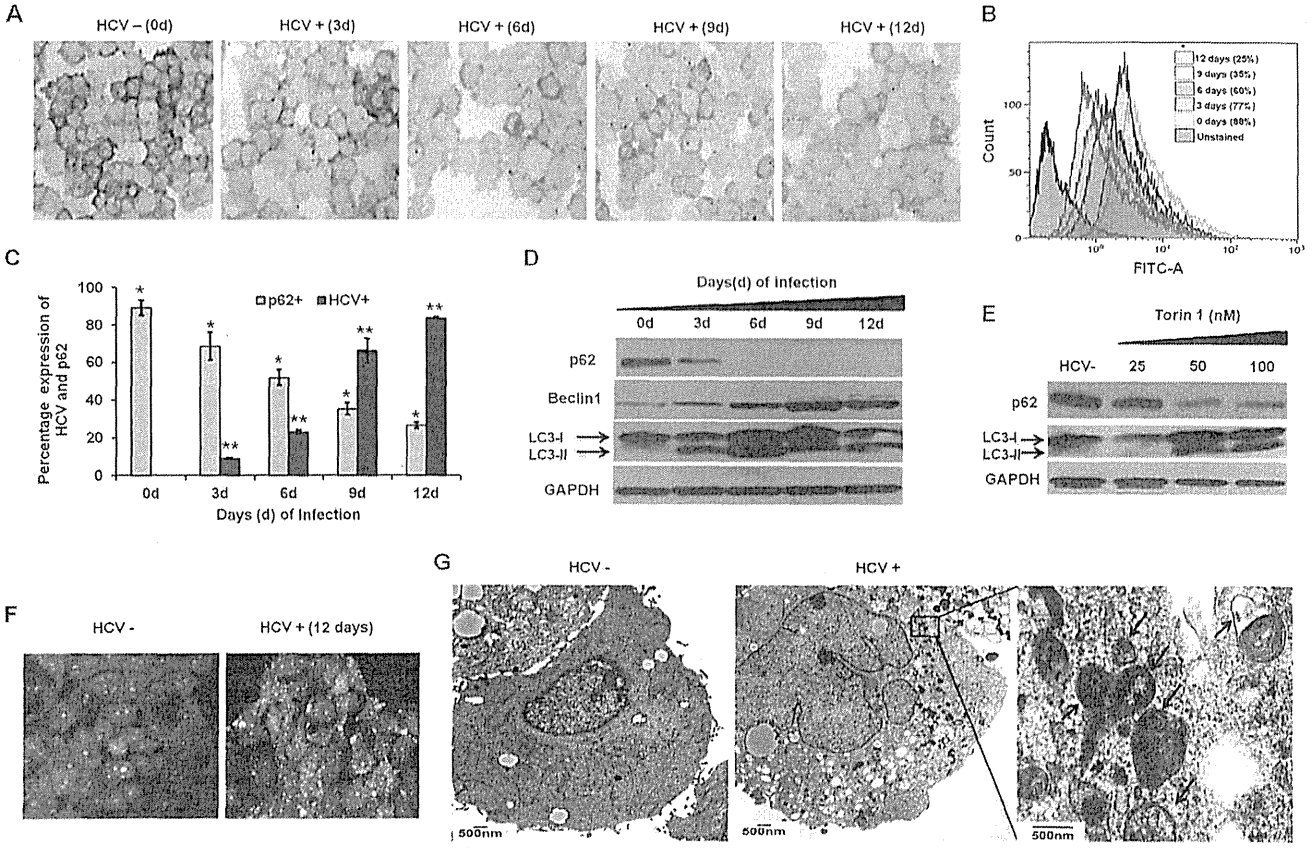

FIG 4 HCV replication induces an autophagy response. (A) Immunostaining for p62 protein in persistently infected Huh-7.5 cells (HCV+) was measured by immunohistochemistry on different days of infection (3 to 12 days). (B) Representative flow cytometry analysis of p62 expression in HCV-infected cells at days 0, 3, 6, 9, and 12 days. A total of 20,000 events were analyzed each time. FITC, fluorescein isothiocyanate. (C) Quantitative analysis of p62 and HCV core expression in HCV-infected cells up to 12 days. Mean percentages from three independent analyses are presented (*, $P < 0.01$; **, $P < 0.001$). (D) Western blot analysis of p62, Beclin 1, and LC3 in HCV-infected cells at different time points. (E) Western blot analysis of p62 and LC3 in uninfected Huh-7.5 cells treated with the autophagy inducer Torin 1. (F) Induction of the autophagy response in an HCV-infected culture was determined after acridine orange staining of autophagolysosomes. In this assay, cells without autophagy induction show green fluorescence, whereas cells with autophagy show accumulation of orange-red cytoplasmic autophagic vacuoles. (G) Uninfected and HCV-infected Huh-7.5 cells were subjected to ultrastructural analysis by transmission electron microscopy (Hitachi H7100). Representative high-power micrographs of autophagic vacuoles (black arrows) present in infected cells show a typical double membrane. The inset box shows double-membrane autophagy vacuoles at a higher magnification.

88% of uninfected Huh-7.5 cells were p62 positive at day 0, and the number of p62-positive cells decreased to 25% on day 12. The experiment was repeated three times, and the mean percentage of cells showing p62 and HCV core expression recorded over 12 days indicated that HCV infection induces an autophagy response. A significant ($P < 0.001$ and $P < 0.0001$) inverse correlation was found between HCV core positivity and p62 negativity in infected Huh-7.5 cells (Fig. 4C). The decreased p62 expression level in HCV-infected Huh-7.5 cells was due to an increase in the autophagy response, as confirmed by Western blotting of Beclin 1 and LC3-II (Fig. 4D). During autophagy, autophagosomes engulf cytoplasmic components, including cytosolic proteins and organelles. The cytosolic form of LC3 (LC3-I) is conjugated to phosphatidylethanolamine to form an LC3-phosphatidylethanolamine conjugate (LC3-II), which is recruited to autophagosomal membranes. Autophagosomes fuse with lysosomes to form autolysosomes, and intra-autophagosomal components are degraded by lysosomal hydrolases. At the same time, LC3-II in the autolysosomal lumen is degraded. Uninfected Huh-7.5 cells treated with the autophagy inducer Torin 1 showed decreased expression levels of p62 and increased expression levels of LC3-II, as determined by Western blotting (Fig. 4E). Induction of autophagy and conversion of LC3-I to LC3-II were increased in infected Huh-7.5 cells and in Huh-7.5 cells treated with Torin 1. Previously, we showed that the induction of the cellular autophagy response increases the number of autophagosomes during HCV infection (20). When the autophagosomes fuse with lysosomes, they form autophagolysosomes, and lysosomal degradation is increased. The presence of induced autophagolysosome formation in the HCV-infected cell culture was confirmed by acridine orange staining under a fluorescence microscope, which showed an increase in the number of orange autophagolysosomes in HCV-infected cells on day 12 (Fig. 4F). The presence of HCV-induced autophagy vacuoles in Huh-7.5 cells with and without viral infection was confirmed at day 12 by transmission electron microscopy (TEM)-based ultrastructural analysis (Fig. 4G). The presence of double-layered membrane vacuoles containing cytoplasmic material (referred to as autophagosomes) was observed in

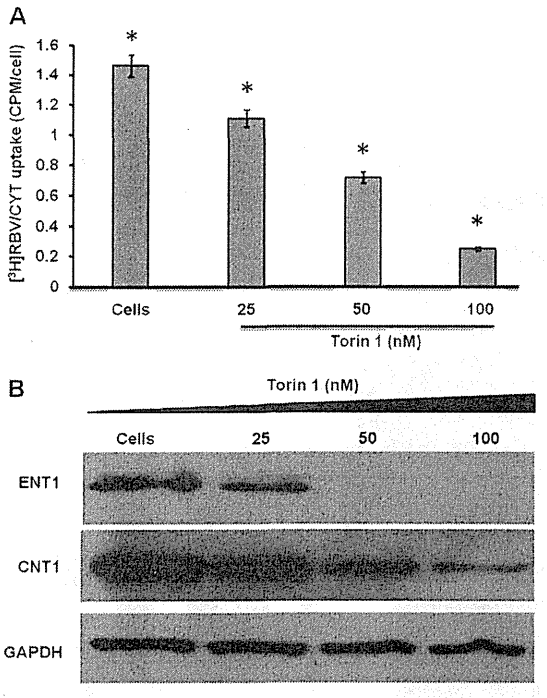

FIG 5 The autophagy inducer Torin 1 impairs RBV uptake and expression of ENT1. Uninfected Huh-7.5 cells were treated with increasing concentrations of Torin 1 for 24 h, and the uptake of ^{3}H-labeled RBV and [^{3}H]cytidine (CYT) was quantified by scintillation counting. (A) [^{3}H]RBV uptake was decreased with increased HCV infection, relative to the control (*, $P < 0.05$). (B) Western blot showing expression levels of ENT1 and CNT1 with increasing concentrations of Torin 1. The GAPDH level was used as an internal control.

HCV-infected cells by electron microscopy. The diameters of putative autophagic vacuoles were found to be in the range of 100 to 500 nm (Fig. 4G, arrows).

To confirm that RBV uptake is directly affected by the cellular autophagy response, we performed an RBV uptake assay with uninfected Huh-7.5 cells in the presence of a known autophagy inducer, Torin 1. These experiments were performed in triplicate. As shown in Fig. 5A, we verified the impairment of RBV uptake in an uninfected Huh-7.5 culture by Torin 1 treatment, with the impairment occurring in a concentration-dependent manner. These results support our hypothesis that increased cellular autophagy significantly impairs RBV uptake ($P < 0.05$) but that the uptake of cytidine is unaffected (Fig. 5A). To verify whether the progressive impairment of RBV uptake in Torin 1-treated cells is due to an increased degradation of ENT1 and CNT1 transporters, cell lysates were prepared from Huh-7.5 cells after 24 h of Torin 1 treatment and examined the expression levels of the ENT1, CNT1, and GAPDH proteins by Western blotting. Torin 1-treated Huh-7.5 cells showed impaired expression of ENT1 and CNT1, but GAPDH protein levels were unaffected (Fig. 5B). These results support the conclusion that the increased autophagy response due to HCV infection impairs RBV uptake through the degradation of the nucleoside transporters ENT1 and CNT1.

Autophagy inhibitors enhance RBV antiviral activity in persistently HCV-infected cell cultures. To determine whether the HCV-induced autophagy response plays a role in impaired HCV clearance by RBV, we performed RBV antiviral assays in triplicate in the presence and absence of different autophagy inhibitors (29). Three autophagy inhibitors, 3-MA, bafilomycin A1 (BafA1), and hydroxychloroquine (HCQ), used in our assays have been shown to block cellular autophagy at multiple steps of autophagolysosome maturation. First, we examined RBV uptake in HCV-infected Huh-7.5 cells in the presence and absence of autophagy inhibitors. As shown in Fig. 6A, the autophagy inhibitors 3-MA and BafA1 significantly improved RBV uptake by HCV-infected Huh-7.5 cells. Second, we examined the mechanisms of improved RBV uptake due to restored expression of ENT1 transporters. As shown in Fig. 6B, the expression level of ENT1 was restored when HCV-infected Huh-7.5 cells were pretreated with each of the different autophagy inhibitors. Western blot analysis showed that p62 expression was restored when HCV-infected Huh-7.5 cells were treated with 3-MA and BafA1, which inhibited autophagy (Fig. 6B). Third, we examined whether cotreatment of HCV-infected cultures with autophagy inhibitors could enhance RBV antiviral activity. However, short-term treatment of HCV-infected cell cultures with 3-MA and BafA1 significantly enhanced the RBV antiviral response ($P < 0.01$) (Fig. 6C). Fourth, the effect of autophagy inhibitor treatments on RBV uptake was verified by immunostaining for HCV core protein in infected cells (Fig. 6D). Finally, an HCV RNA titer was determined by using RT-qPCR, to ensure that the additive inhibitory effect of RBV and autophagy inhibitors was also reflected in viral RNA levels. The results showed that BafA1 alone and in combination with RBV significantly decreased HCV RNA levels ($P < 0.01$) (Fig. 6E).

Long-term treatment by a combination of RBV and HCQ induces HCV clearance. A cause-effect relationship between the induction of autophagy and blockage of the RBV antiviral response was further established by applying a long-term combination treatment with an autophagy inhibitor (HCQ) and RBV in a persistently infected Huh-7.5 cell culture. Infected Huh-7.5 cells were treated with viable doses of HCQ (10 μM), alone and in combination with RBV. Three consecutive treatments with HCQ (both alone and in combination with RBV) were performed at 48-h intervals, and HCV clearance was determined by *Renilla* luciferase activity. These experiments were performed in triplicate.

As shown in Fig. 7A, HCQ along with RBV significantly inhibited *Renilla* luciferase activity, compared with cells treated with either RBV alone or HCQ alone. In our study of HCV-infected Huh-7.5 cells treated with HCQ alone, *Renilla* luciferase and HCV RNA levels were significantly reduced (Fig. 7A and B). Two explanations are possible for the observed inhibition. The HCQ inhibitory effect could be due to either the inhibition of viral spread or the inhibition of autophagy. We cannot rule out the possibility that some of the HCQ antiviral action resides at the level of inhibition of new viral infection and its spread. However, our data also support that the inhibitory effect of HCQ is due to inhibition of autophagy, as Western blot analysis showed that the expressions of ENT1, p62, and the clathrin heavy chain were restored (Fig. 7C and D). The clearance of HCV replication in the culture by combined treatment with RBV and HCQ was confirmed by HCV core immunostaining (Fig. 7E). The expression of HCV core protein was undetectable after the third treatment. These results provide evidence that the HCV-induced autophagy response impairs RBV antiviral activity.

Flow sorting confirms that RBV resistance to HCV-positive cultured cells shows impaired expression of ENT1 and clathrin. To verify that the absence of ENT1 expression in HCV-infected

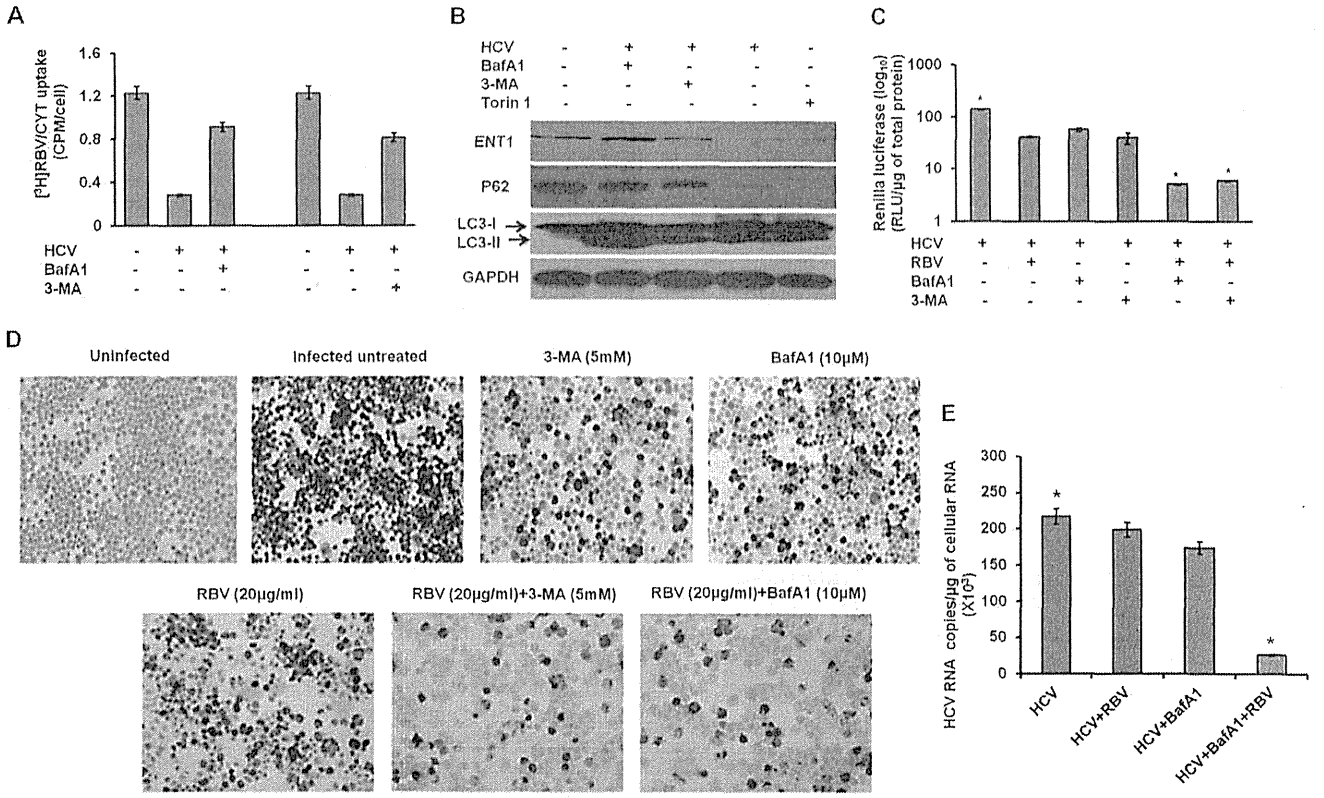

FIG 6 Inhibition of the autophagy response by autophagy inhibitors rescues RBV uptake and expression of ENT1 and enhances antiviral activity. (A) Levels of [^{3}H]RBV and [^{3}H]cytidine (CYT) (control) uptake in HCV-infected cultures on day 3 were determined in the presence and absence of the autophagy inhibitors 3-MA and BafA1. (B) Western blot showing expression of ENT1, p62, LC3, and GAPDH in HCV-infected Huh-7.5 cells after treatment with the autophagy inhibitors 3-MA and BafA1 for 24 h. (C) *Renilla* luciferase levels in HCV-infected cells quantifying RBV antiviral activity in the presence and absence of autophagy inhibitors (3-MA and BafA1). Equal numbers of HCV-infected cells were treated with RBV (20 μg/ml), 3-MA (5 mM), and BafA1 (10 μM), alone and in combination, for 24 h. After 24 h, cells were harvested, to measure *Renilla* luciferase-assessed HCV replication in the treated culture. (D) HCV-infected cells were treated with RBV (20 μg/ml), 3-MA (5 mM), and BafA1 (10 μM), alone and in combination, for 24 h. After 24 h, HCV core protein expression was measured by immunostaining. (E) HCV RNA levels in an infected culture treated with BafA1 alone and in combination with RBV (*, $P < 0.05$).

cultures is associated with impaired antiviral activity, we separated HCV-positive and HCV-negative cells in persistently infected Huh-7.5 cultures by fluorescence-activated cell sorting (FACS) after HCV core staining. Infected cells were treated with RBV on day 13 (T1) and day 16 (T2), and cell sorting was done on day 19 (Fig. 8A). *Renilla* luciferase activity showed that RBV antiviral activity was impaired in HCV-infected cultures (Fig. 8B). The flow-sorting experiments performed on day 19 indicate that RBV treatment did not decrease the number of HCV core-positive cells (Fig. 8C). The flow-sorting experiments were repeated three times on day 19, and the difference between the average mean percentages of HCV core-positive cells with and those without RBV treatment was found not to be significant (Fig. 8D). Protein extracts of sorted cells (HCV-positive and HCV-negative Huh-7.5 cells) were examined for the expression of ENT1 and CNT1 by Western blotting. Only HCV-positive cells showed downregulated ENT1 expression (Fig. 8E). The expression of GAPDH remained at comparable levels in HCV-positive and HCV-negative lysates. Previous studies have verified that the expression of ENT1 on the plasma membrane is regulated by clathrin-mediated endocytosis (30). Expression of clathrin heavy chains was examined by Western blotting using flow-sorted HCV-infected Huh-7.5 cells. Interestingly, the expression of the clathrin heavy chain was impaired in persistently HCV-infected Huh-7.5 cells (Fig. 8E).

The HCV-induced autophagy response leads to degradation of the clathrin heavy chain. Equilibrative nucleoside transporters are expressed on the plasma membrane of hepatocytes, internalized by clathrin-mediated endocytosis, and then recycled back to the plasma membrane for subsequent use or otherwise subjected to lysosomal degradation. A recent study showed that the clathrin molecule is required for both autophagolysosome formation and autophagic lysosome reformation (30). The role of clathrin in autophagy is also supported by a number of studies showing that plasma membranes contribute to the formation of preautophagosomes, indicating that the expression of plasma membrane protein could also be regulated by autophagy (31). The N terminus of the clathrin heavy chain interacts with ATG16L1 and is involved in the formation of the structure of preautophagolysosomes and the inhibition of clathrin-mediated internalization. Expression of the clathrin heavy chain decreases the ATG16L1 protein level (31). Based on these reports, we verified the expressions of the clathrin heavy chain, ATG16L1, and GAPDH by Western blotting after HCV infection of Huh-7.5 cells over 12 days. Clathrin heavy chain expression was impaired in HCV-infected cells, whereas

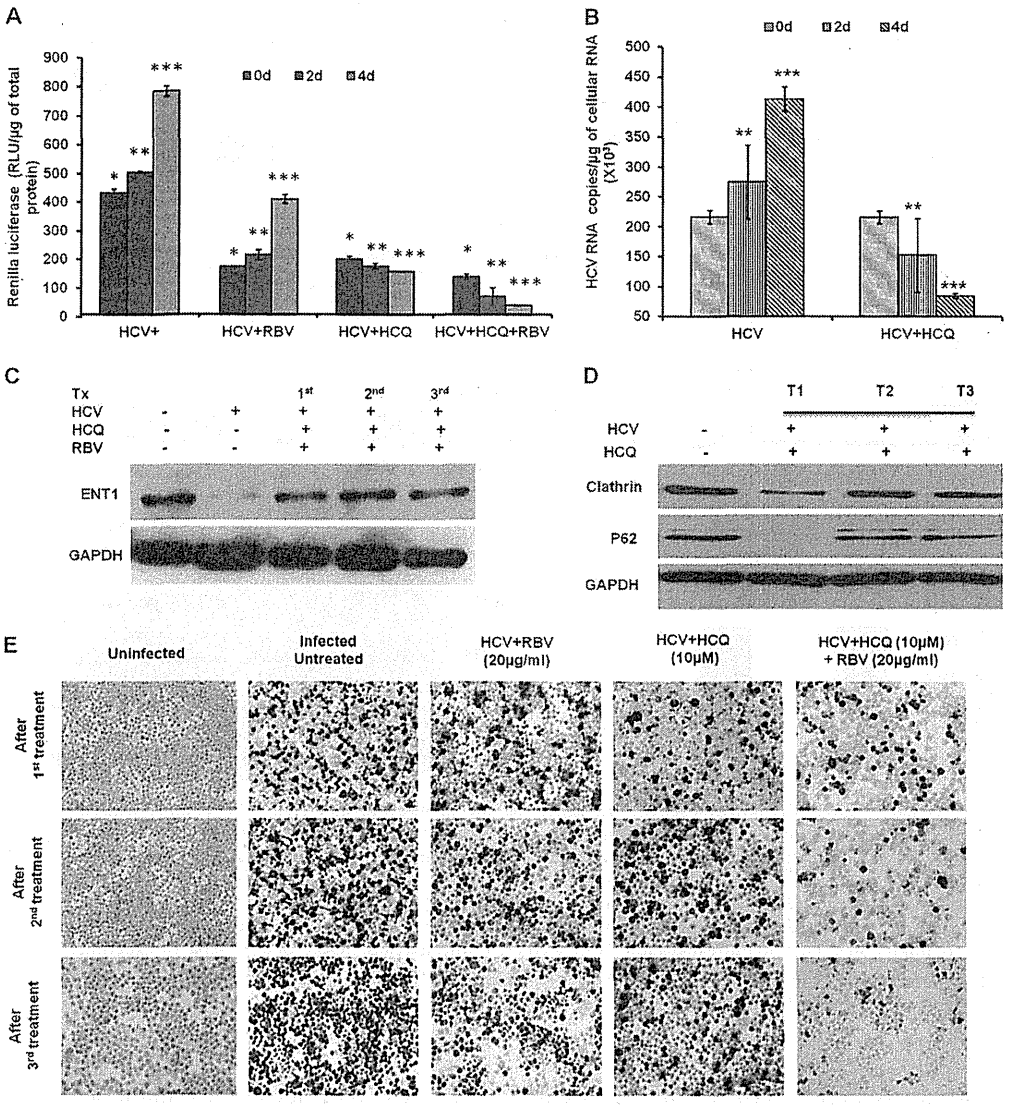

FIG 7 Long-term treatment of a persistently HCV-infected culture with the combination of an autophagy inhibitor, HCQ, and RBV induces HCV clearance by restoring ENT1 expression. (A) HCV-infected cells were given three consecutive treatments (Tx) with RBV (20 μg/ml) and HCQ (10 μM), alone and in combination. Every 2 days, the cells were harvested, and HCV replication was measured by measuring *Renilla* luciferase activity (*, $P < 0.05$; **, $P < 0.001$; ***, $P < 0.0001$). (B) HCV RNA levels in untreated HCV-infected cells and HCV-infected cells treated with HCQ are shown for comparison (**, $P < 0.001$; ***, $P < 0.0001$). (C) ENT1 protein levels were measured by Western blotting. (D) Western blots showing clathrin heavy chain, p62, and GAPDH in an HCQ-treated culture (T1, T2, and T3 represent the treatments). (E) The antiviral activity of combination treatment with HCQ and RBV was assessed by measurement of HCV core protein expression by immunohistochemistry.

ATG16L1 expression increased (Fig. 9A); HCV expression in infected cultures impaired clathrin heavy chain expression, as determined by colocalization experiments in which clathrin was detected with a green fluorescence probe and the HCV core was detected by using a red fluorescence probe (Fig. 9B). A real-time RT-qPCR assay was used to determine the effects of HCV infection on clathrin heavy chain mRNA levels; levels were significantly increased in HCV-infected cultures compared with the levels in uninfected Huh-7.5 cells (Fig. 9C). Western blot analysis demonstrated downregulation of clathrin in uninfected Huh-7.5 cells treated with Torin 1, confirming that the autophagy response diminishes clathrin heavy chain expression (Fig. 9D). Uninfected Huh-7.5 cells treated with Torin 1 showed reduced clathrin heavy chain expression, as determined by immunofluorescence microscopy (Fig. 9E).

Silencing of the clathrin heavy chain impairs membrane expression of an ENT1-GFP chimera. A previous study demonstrated that human ENT1 is trafficked to the plasma membrane in association with microtubules and is then recycled by clathrin-mediated endocytosis (23). A chimeric clone of ENT1 and a green fluorescent protein developed in the laboratory of Imogen Coe were used to verify how the HCV-induced autophagy response alters cell surface expression of ENT1 through the clathrin heavy chain. Huh-7.5 cells transfected with ENT1-GFP plasmids showed that the protein was predominantly expressed on the plasma membrane on day 4 (Fig. 10A) and that RBV treatment had no

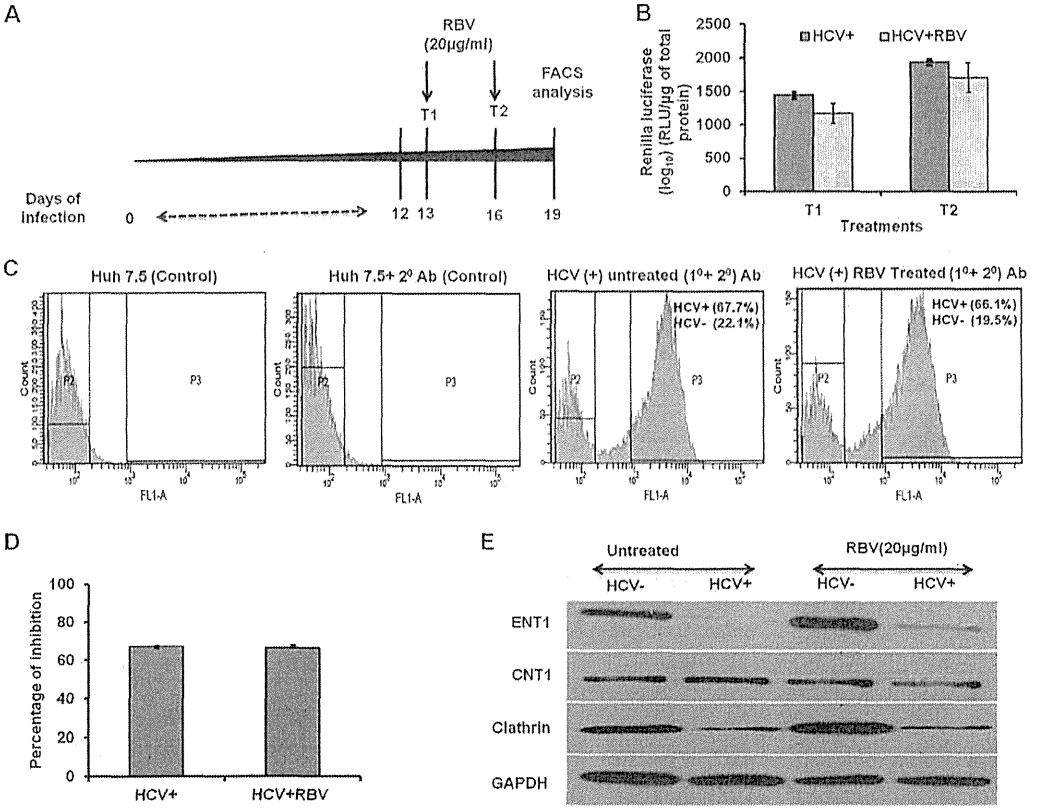

FIG 8 Flow sorting verifies that impaired RBV antiviral activity against HCV is due to low expression levels of ENT1 and the clathrin heavy chain. (A) Diagram showing the experimental design for RBV treatment and flow sorting of an HCV-infected culture. HCV-infected Huh-7.5 cells at 12 days after infection received two consecutive treatments (T1 and T2) on the 13th and 16th days with RBV (20 μg/ml) and were then subjected to flow analysis (19th day). (B) *Renilla* luciferase activity of an HCV-infected culture with or without RBV treatment (T1 and T2). (C) Flow-sorted cells showing the presence of core-expressing cells in HCV-infected untreated and RBV-treated Huh-7.5 cells. Intracellular core protein expression was detected by an immunofluorescence technique using a green fluorescence secondary antibody and then detected by flow cytometry. Infected Huh-7.5 cells with only secondary antibody (Huh-7.5 + 2^0 Ab) were used as a control. (D) Percentage of inhibition of HCV in untreated and RBV-treated HCV-infected cells. Results of three separate experiments are summarized as mean percentages of inhibition of HCV-expressing cells with or without RBV. (E) Western blot analysis showing the expressions of ENT1, CNT1, and CHC between RBV-treated sensitive and resistant populations. The GAPDH level in the lysate was used as an internal control.

effect on membrane expression (Fig. 10B). We then verified that autophagy induction by Torin 1 treatment or HCV infection abolishes ENT1-GFP membrane expression in Huh-7.5 cells (Fig. 10C and D). Confocal microscopy showed that membrane expression of ENT1-GFP in uninfected Huh-7.5 cells remained unaltered, whereas cells expressing HCV core protein only altered ENT1-GFP expression (Fig. 10E). Taken together, these results confirm that autophagy induction abolishes cell surface expression of ENT1-GFP through lysosomal degradation.

We then verified whether silencing of the clathrin heavy chain could have a similar effect on ENT1, CNT1, and ATG16L1 expression in Huh-7.5 cells. Cells were transfected individually with siRNAs for clathrin and ATG16L1 and with a scrambled siRNA by using Lipofectamine 2000. After 72 h, cell lysates were examined for clathrin, ATG16L1, ENT1, ENT2, and CNT1 expression by Western blotting. The experiment showed that silencing of the clathrin heavy chain decreased the expression levels of ATG16L1 and ENT1 but not that of ENT2 (Fig. 10F). The decrease in the ENT1 expression level in clathrin-silenced Huh-7.5 cells indicates that clathrin is required for the recycling of ENT1 and that ENT1 undergoes forced degradation in the absence of the clathrin heavy chain (30). Silencing of the clathrin heavy chain did not affect CNT1 transporter levels, as determined by Western blotting. Silencing of ATG16L1 did not alter clathrin heavy chain or ENT1 expression levels (Fig. 10F). Silencing of the clathrin heavy chain, but not of ATG16L1, also abolished cell surface expression of ENT1-GFP in uninfected Huh-7.5 cells (Fig. 10G). The results of these experiments indicate that clathrin heavy chain expression is required for hepatocyte membrane expression of the ENT1-GFP chimera.

Decreased expression levels of the clathrin heavy chain and ENT1 in HCV-infected primary hepatocytes and in liver biopsy samples from chronic HCV patients. The significance of our cell culture findings was further validated by using HCV-infected primary human hepatocytes (PHHs) as well as liver biopsy samples from patients with chronic HCV. We established an HCV replication model using PHHs and found that HCV replication in PHHs can be inhibited by IFN-α. Using this system, we verified HCV replication accompanying PHH-induced ER stress and the autophagy response but impaired expression of IFNAR1, IFNγR1, and RBV transporters. Expression of the IFN-λ receptor was not affected by ER stress or the autophagy response. In a previous

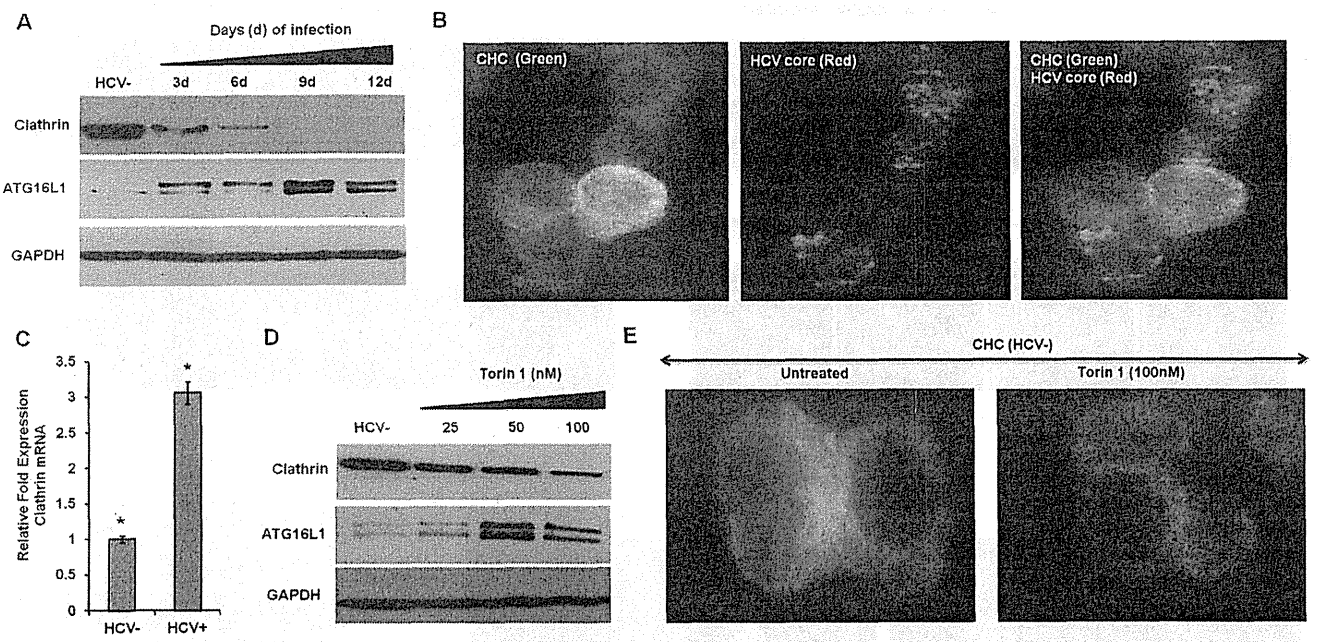

FIG 9 HCV infection induces degradation of the clathrin heavy chain. (A) Western blot analysis of clathrin heavy chain and ATG16L1 protein levels in HCV-infected Huh-7.5 cells. GAPDH levels were used as an internal control. (B) Immunofluorescence staining of HCV core-positive (red) HCV-infected Huh-7.5 cells showing negative expression of the clathrin heavy chain (green). (C) Real-time RT-qPCR showing the fold changes of clathrin mRNA levels after HCV infection. (D) Induction of autophagy in Huh-7.5 cells by Torin 1 shows decreased expression levels of the clathrin heavy chain by Western blotting. (E) Huh-7.5 cells treated with a known autophagy inducer, Torin 1 (100 nM), show decreased expression levels of the clathrin heavy chain (green) by fluorescence microscopy.

study, we verified ER stress- and autophagy-mediated degradation of both IFNAR1 and RBV transporter expression using liver biopsy samples from patients with chronic HCV infection (32). We showed that markers of ER stress and autophagy are induced in chronically HCV-infected liver tissues. Primary hepatocytes were infected with the JFH-ΔV3-Rluc chimera virus at an MOI of 0.1. The expression levels of clathrin, ENT1, and CNT1, and HCV core in infected PHHs were measured by Western blotting. The results indicated that on day 8, expressions of clathrin, ENT1, and CNT1 were undetectable (Fig. 11A). Expression levels of clathrin, ENT1, and CNT1 were negatively correlated with HCV core expression, as determined by Western blotting. The expression levels of the clathrin heavy chain, ENT1, and CNT1 were examined by using limited amounts of tissue extracts from liver biopsy specimens of patients with chronic HCV infection and control normal livers (Fig. 11B). In summary, we were able to verify the significance of our experimental findings in a study on an *in vitro* HCV-infected cell culture system.

Based on the results presented above, we propose a model of how ENT membrane expression and recycling are affected by an autophagy response induced by HCV infection through the clathrin heavy chain (Fig. 12). In uninfected cells, the clathrin heavy chain regulates ENT1 membrane expression. In HCV-infected cells, membrane proteins are degraded due to autophagy, leading to defective clathrin-mediated endocytosis. Chronic HCV infection downregulates the clathrin heavy chain, and in the absence of the clathrin heavy chain, ENT1 is forced into the lysosomal degradation pathway.

DISCUSSION

Ribavirin has been used as an antiviral drug in the treatment of a number of viruses, including HCV, RSV, and LASV. Ribavirin monotherapy is not very effective (33, 34); however, RBV in combination with IFN-α shows a significant improvement in the HCV treatment response. The results from recent clinical trials suggest that RBV may remain an essential component of HCV treatment in combination with new DAAs to prevent relapse (4). An understanding of the mechanisms of RBV antiviral action and resistance could lead to novel strategies for improving its antiviral efficacy against HCV as well as against other viruses. In this study, we showed that RBV antiviral activity is blocked due to an induced autophagy response in HCV-infected cell cultures. These results based on cell culture experiments are consistent with clinical findings, where it has been observed that individuals with high viral titers are more resistant to combination therapy with IFN-α and RBV (34). The mechanism of impaired RBV antiviral activity in persistently HCV-infected cells is related to the reduced expression of ENT1, an RBV transporter, and the reduced uptake of RBV is in agreement with the results of other research reported previously (14–17).

Autophagy is a cellular degradation process essential for cell survival during HCV infection. The cellular autophagy process plays an important role in persistent viral infection, as it can modulate innate antiviral immunity as well as antiviral drug resistance. The autophagy process is maintained in patients with chronic liver disease due to both viral and nonviral causes (35). The HCV-induced autophagy response degrades the ENT1 protein without affecting mRNA levels in infected Huh-7.5 cells. The autophagy